Communications in Analysis and Mechanics

https://www.aimspress.com/journal/cam

Communications in Analysis and Mechanics, 18(2): 476–510.
DOI: 10.3934/cam.2026020
Received: 21 September 2025
Revised: 12 February 2026
Accepted: 26 March 2026
Published: 18 June 2026

Research article

Two-grid mixed virtual element method for a nonlinear fourth-order time-fractional reaction-diffusion equation

Jianmei Chen, Xinyuan Liu and Yang Liu*

School of Mathematical Sciences, Inner Mongolia University, Hohhot 010030, China

* **Correspondence:** Email: mathliuyang@imu.edu.cn.

Abstract: In this article, we developed a two-grid mixed virtual element method (MVEM) for solving a time-dependent fourth-order reaction-diffusion equation with a Riemann-Liouville fractional derivative and a nonlinear reaction term. By introducing an auxiliary variable $\sigma = \Delta u$, we reformulated the problem into a coupled system of second-order equations. Then we discretized the equations at $t_{k-\frac{\alpha}{2}}$ by a second-order backward differentiation formula (BDF2) with a fractional parameter α. The method employed a two-grid strategy: First, we solved a nonlinear problem via Newton iterations on a coarse ploygonal grid, and subsequently, leveraging the coarse-grid solutions, we solved a linearized problem on a fine virtual element space. We established the stability of this method and derived a priori L^2-norm error estimates with the optimal convergence result $O(\Delta t^2 + h^{k+1} + H^{2k+2})$, where Δt denotes the time step size, h and H are the fine and coarse spatial mesh sizes, respectively, and k is the polynomial degree of the virtual element space. Numerical experiments validated the theoretical convergence rates, and it was demonstrated that applying the two-grid MVEM is computationally more efficient than solving the nonlinear system directly on the fine grid.

Keywords: two-grid mixed virtual element method; fourth-order time-fractional reaction-diffusion equation; a priori error analysis in L^2-norm; unstructured meshes
Mathematics Subject Classification: 65N30, 65M60

1. Introduction

Fourth-order partial differential equations are widely employed in scientific and engineering fields. Theoretical studies [1,2] and numerical analysis [3] for fourth-order problems have been well-established. In recent years, nonlinear fourth-order time-fractional parabolic equations have attracted considerable interest due to their exceptional capacity to model complex physical phenomena across multiple disciplines [4, 5].

Our work focuses on the following nonlinear fourth-order reaction-diffusion equation with a Riemann-Liouville fractional derivative:

$$\frac{\partial u}{\partial t} - \frac{\partial^\alpha \Delta u}{\partial t^\alpha} - \Delta u + \Delta^2 u = f(u) + g(\mathbf{x}, t), \quad (\mathbf{x}, t) \in \Omega \times J, \tag{1.1}$$

with Dirichlet boundary conditions

$$u(\mathbf{x}, t) = \Delta u(\mathbf{x}, t) = 0, \quad (\mathbf{x}, t) \in \partial\Omega \times J, \tag{1.2}$$

and the initial condition

$$u(\mathbf{x}, 0) = u_0(\mathbf{x}), \quad \mathbf{x} \in \Omega, \tag{1.3}$$

where Ω is a bounded Lipschitz domain of $\mathbb{R}^2$ with boundary $\partial\Omega$, $J = (0, T]$ is the time interval, and $g(\mathbf{x}, t)$ is an external forcing function. The nonlinear source term $f(u)$ is a locally Lipschitz continuous function, satisfing $|f(u)| + |f'(u)| + |f''(u)| \leq M$ in Ω, where M is a positive constant. The left Riemann-Liouville fractional derivative $\frac{\partial^\alpha \Delta u}{\partial t^\alpha}$ is defined by

$$\frac{\partial^\alpha \Delta u(\mathbf{x}, t)}{\partial t^\alpha} = \frac{1}{\Gamma(1-\alpha)} \frac{\partial}{\partial t} \int_0^t \frac{\Delta u(\mathbf{x}, s)}{(t-s)^\alpha} ds, \quad 0 < \alpha < 1. \tag{1.4}$$

The equations including time-fractional derivative $\frac{\partial^\alpha (\Delta u)}{\partial t^\alpha}$ and fourth-order spatial derivative $\Delta^2 u$ can effectively describe nonlocal memory effects and high-order energy dissipation mechanisms [6]. However, these terms along with a nonlinear term introduce great computational challenges. The nonlocality of $\frac{\partial^\alpha \Delta u}{\partial t^\alpha}$ generates dense temporal discretization matrices, escalating memory costs; the stiffness induced by $f(u)$ imposes restrictive CFL-type stability conditions on explicit schemes; and $\Delta^2 u$ requires high-order spatial discretization schemes to amplify computational complexity. These challenges have motivated many scholars to apply some numerical methods to obtain efficient solutions, such as finite difference methods (FDMs) [5, 7, 8], finite element methods (FEMs) [9], spectral methods [10], collocation methods [11, 12], meshless methods [13], and so on.

For solving partial differential equations (PDEs) on general polygonal and polyhedral meshes, Beirão da Veiga et al. [14, 15] proposed the virtual element method (VEM), which has emerged as a powerful numerical method. By projecting onto polynomial subspaces, the VEM constructs approximation spaces without requiring explicit basis functions, thus offering significant flexibility for high-order formulations and complex geometries. Brezzi et al. [16] extended this framework to mixed virtual element methods (MVEMs) for the discretization of $H(\text{div})$-conforming vector fields, while subsequent advancements adapted the VEM for parabolic PDEs [17], nonlinear parabolic problems [18], and nonlinear fourth-order PDEs [19–21]. Zhang and Feng [22] used the MVEM to study the time-fractional fourth-order subdiffusion equation. To improve the computational efficiency of the VEM in solving the nonlinear PDEs, we introduce the two-grid FEM pioneered by Xu [23, 24] and applied by other authors in [9, 25–28], which can enhance computing efficiency by solving nonlinear problems on a coarse grid and linearized equations on a fine grid.

Based on the above considerations, we propose a two-grid MVEM with a second-order time approximation technique to quickly solve (1.1). The main contributions of this work are summarized as follows:

- We introduce an auxiliary variable $\sigma = \Delta u$ to reformulate the fourth-order system into a nonstandard mixed weak formulation, and then formulate a fully discrete nonstandard MVEM with the second-order time approximation at $t_{k-\frac{\alpha}{2}}$ [6,29]. To improve the computing efficiency for the fully discrete nonstandard MVEM, we develop a fast fully discrete two-grid MVEM.
- We provide stability analysis and derive optimal L^2-norm error estimates for the fully discrete nonstandard MVEM. We prove the stability for the fully discrete fast two-grid MVEM and derive the L^4-norm estimate based on the virtual element space. Further, we present optimal L^2-norm error estimates for the fully discrete fast two-grid MVEM, which are derived based on the L^4-norm estimate.
- We carry out numerical experiments to verify the accuracy and computing efficiency of the two-grid MVEM. The numerical results show that the developed two-grid MVEM can reduce computing time.

The layout of this article is organized as follows. In Section 2, we introduce an auxiliary variable $\sigma = \Delta u$, and obtain the mixed weak formulation and VEM approximation of the nonlinear fourth-order reaction-diffusion equation. In Section 3, we develop a fully discrete two-grid MVEM and carry out the stability analysis. In Section 4, we derive optimal L^2-norm error estimates based on the coarse and fine grids. In Section 5, we carry out numerical tests to examine the validity and computing efficiency of our two-grid MVEM. In Section 6, we provide discussions for the conclusion and future advancements.

2. MVEM approximation

2.1. The mixed weak formulation

We introduce an auxiliary variable $\sigma = \Delta u$, and reformulate (1.1)–(1.3) as the following coupled system:

$$\begin{cases} \frac{\partial u}{\partial t}(\mathbf{x},t) - \frac{\partial^\alpha \Delta u}{\partial t^\alpha}(\mathbf{x},t) - \Delta u(\mathbf{x},t) + \Delta\sigma(\mathbf{x},t) = f(u) + g(\mathbf{x},t), \quad (\mathbf{x},t) \in \Omega\times J, \\ \sigma(\mathbf{x},t) - \Delta u(\mathbf{x},t) = 0, \quad (\mathbf{x},t)\in\Omega\times J, \\ u(\mathbf{x},t) = \sigma(\mathbf{x},t) = 0, \quad (\mathbf{x},t)\in\partial\Omega\times J, \\ u(\mathbf{x},0) = u_0(\mathbf{x}), \quad \mathbf{x}\in\Omega. \end{cases} \tag{2.1}$$

The mixed weak formulation of (2.1) reads: find $u(\mathbf{x},t), \sigma(\mathbf{x},t) \in L^2((0,T], H_0^1(\Omega))$, such that for $t \in J$,

$$\begin{cases} (\frac{\partial u}{\partial t}(\mathbf{x},t), v) + a(\frac{\partial^\alpha u}{\partial t^\alpha}(\mathbf{x},t), v) + a(u(\mathbf{x},t),v) - a(\sigma(\mathbf{x},t),v) = (f(u),v) + (g(\mathbf{x},t),v), \forall v\in H_0^1(\Omega), \\ (\sigma(\mathbf{x},t),w) + a(u(\mathbf{x},t),w) = 0, \forall w \in H_0^1(\Omega), \end{cases} \tag{2.2}$$

where $u_0(\mathbf{x}), g(\mathbf{x},t) \in C(\bar{\Omega})$, $(\cdot,\cdot)$ is the scalar product in $L^2(\Omega)$, and $a(\cdot,\cdot)$ is defined by

$$a(u,v) := \int_\Omega \nabla u \nabla v d\mathbf{x} \tag{2.3}$$

with $|v|_1^2 = a(v,v)$.

Remark 1. *We introduce the auxiliary variable $\sigma = \Delta u$ to reformulate the fourth-order problem into a second-order mixed system. By retaining Δu within the fractional derivative term, we obtain the nonstandard mixed weak formulation* (2.2). *If we replace Δu with σ in the fractional derivative* *term and the second-order term, we obtain the following standard mixed weak formulation: find* $u(\mathbf{x}, t), \sigma(\mathbf{x}, t) \in L^2((0, T], H_0^1(\Omega))$*, such that for* $t \in J$*,*

$$\begin{cases} (\frac{\partial u}{\partial t}(\mathbf{x}, t), v) - (\frac{\partial^\alpha \sigma}{\partial t^\alpha}(\mathbf{x}, t), v) - (\sigma(\mathbf{x}, t), v) - a(\sigma(\mathbf{x}, t), v) = (f(u), v) + (g(\mathbf{x}, t), v), \forall v \in H_0^1(\Omega), \\ (\sigma(\mathbf{x}, t), w) + a(u(\mathbf{x}, t), w) = 0, \forall w \in H_0^1(\Omega). \end{cases} \tag{2.4}$$

In this work, we focus on the nonstandard mixed weak formulation (2.2).

2.2. VEM space and projection operators

Let $\mathcal{T}_h$ denotes a family of finite polygon decomposition meshes for the domain $\Omega \subset \mathbb{R}^2$, where $\bar{\Omega} = \cup_{K \in \mathcal{T}_h} \bar{K}$, $h = \max_{K \in \mathcal{T}_h} h_K$, and h_K is the diameter of K. Denote ε_h as a family of edges of $\mathcal{T}_h$. Consider the following additional assumptions provided in [14, 17]: There exists a constant $\rho > 0$, such that for every element $K \in \mathcal{T}_h$,

- K is star-shaped with respect to a ball of radius $\geq \rho h_K$.
- The distance between any two vertices of K is $\geq \rho h$.
- For all $e \subset \partial K$, it holds that $h_e \geq \rho h_K$.

For all $K \in \mathcal{T}_h$, let $k \in \mathbb{N}, k \geq 1$, $\mathbb{P}_k(K)$ is the space of polynomials with degree $\leq k$ on K, and the augmented local function space V_h^K is defined by

$$V_h^K = \left\{ v_h \in H^1(K) \cap C^0(K) : v_h|_e \in \mathbb{P}_k(e), \forall e \in \partial K, \Delta v_h \in \mathbb{P}_k(K) \right\}.$$

We introduce the broken Sobolev space

$$H^s(\mathcal{T}_h) = \prod_{K \in \mathcal{T}_h} H^s(K) = \left\{ v \in L^2(\Omega) : v|_K \in H^s(K) \right\}, \forall s > 0$$

with the broken H^s-norm and H^s-seminorm defined by

$$\|v\|_{s,\mathcal{T}_h}^2 = \sum_{K \in \mathcal{T}_h} \|v\|_{s,K}^2, \ v \in H^s(\mathcal{T}_h), \quad |v|_{1,\mathcal{T}_h}^2 = \sum_{K \in \mathcal{T}_h} \|\nabla v\|_{0,K}^2, \ v \in H^1(\mathcal{T}_h). \tag{2.5}$$

The inner product $(\cdot, \cdot)$ and the bilinear form $a(\cdot, \cdot)$ can be split as

$$(u, v) = \sum_{K \in \mathcal{T}_h} (u, v)_K, \quad a(u, v) = \sum_{K \in \mathcal{T}_h} a^K(u, v). \tag{2.6}$$

The local projection operator $\Pi_{K,k}^\nabla$: $V_h^K \mapsto \mathbb{P}_k(K)$ is defined as

$$\begin{cases} a^K\left(\Pi_{K,k}^\nabla v_h, q\right) = a^K(v_h, q), \quad \forall q \in \mathbb{P}_k(K), \\ P_0\left(\Pi_{K,k}^\nabla v_h\right) = P_0 v_h, \end{cases} \tag{2.7}$$

where P_0 is defined by

$$P_0 v_h := \frac{1}{n(K)} \sum_{i=1}^{n(K)} v_h(V_i), \ k = 1, \quad P_0 v_h := \frac{1}{|K|} \int_K v_h \mathrm{d}x, \ k \geq 2. \tag{2.8}$$

Define the local virtual space as

$$\tilde{V}_h^K = \left\{ v_h \in V_h^K : \int_K \left(\Pi_{K,k}^{\nabla} v_h\right) q \, \mathrm{d}x = \int_K v_h q \, \mathrm{d}x, \forall q \in \mathbb{P}_k/\mathbb{P}_{k-2}(K) \right\},$$

where $\mathbb{P}_k/\mathbb{P}_{k-2}(K)$ denotes the L^2-orthogonal complement space of $\mathbb{P}_{k-2}(K)$ in $\mathbb{P}_k(K)$. The local L^2 projection operator $\Pi_{K,k}^0 : \tilde{V}_h^K \mapsto \mathbb{P}_k(K)$ is defined as

$$\left(\Pi_{K,k}^0 v_h, q\right)_K = (v_h, q)_K, \quad \forall q \in \mathbb{P}_k(K). \tag{2.9}$$

It is evident that these two projection operators have the following estimations:

$$\|\Pi_{K,k}^0 v\|_K \le \|v\|_K, \quad |\Pi_{K,k}^{\nabla} v|_{1,K} \le |v|_{1,K}, \tag{2.10}$$

and for the projection operator $\Pi_{K,k}^0$, it holds that

$$\left\|v - \Pi_{K,k}^0 v\right\|_K + h_K \left|v - \Pi_{K,k}^0 v\right|_{1,K} \le C_\pi h_K^s |v|_{s,K}, \forall v \in H^m(K), \ 1 \le s \le k+1. \tag{2.11}$$

Therefore, according to a set of $\tilde{V}_h^K$, the global virtual spaces are given by

$$\tilde{V}_h = \left\{ v \in H_0^1(\Omega) : v|_K \in \tilde{V}_h^K, \forall K \in \mathcal{T}_h \right\}.$$

Based on the projection operators $\Pi_{K,k}^0$ and $\Pi_{K,k}^{\nabla}$, we can introduce two computable, locally supported discrete bilinear forms $m_h^K(\cdot,\cdot) : \tilde{V}_h^K \times \tilde{V}_h^K \mapsto \mathbb{R}$ and $a_h^K(\cdot,\cdot) : \tilde{V}_h^K \times \tilde{V}_h^K \mapsto \mathbb{R}$ from [14]

$$\begin{aligned} m_h^K(u_h, v_h) &= (\Pi_{K,k}^0 u_h, \Pi_{K,k}^0 v_h)_K + S_m^K(u_h - \Pi_{K,k}^0 u_h, v_h - \Pi_{K,k}^0 v_h), \\ a_h^K(u_h, v_h) &:= a^K(\Pi_{K,k}^{\nabla} u_h, \Pi_{K,k}^{\nabla} v_h) + S_a^K(u_h - \Pi_{K,k}^{\nabla} u_h, v_h - \Pi_{K,k}^{\nabla} v_h), \end{aligned}$$

where $S_m^K = S^K, S_a^K = h_K^{-2} \cdot S^K$,

$$S^K(u_h, v_h) := \sum_{j=1}^{N^K} \mathrm{dof}_j(u_h) \cdot \mathrm{dof}_j(v_h).$$

For all $K \in \mathcal{T}_h$, the bilinear forms satisfy the following properties:

- k-consistency: for all $q \in \mathbb{P}_k(K)$ and $v_h \in \tilde{V}_h^K$,

$$m_h^K(q, v_h) = (q, v_h)_K, \quad a_h^K(q, v_h) = a^K(q, v_h), \tag{2.12}$$

- stability: there are positive constants $\underset{\sim}{\mathfrak{I}}, \tilde{\mathfrak{I}}, \underset{\sim}{\xi}$, and $\tilde{\xi}$ independent of h, such that for $v_h \in \tilde{V}_h^K$,

$$\underset{\sim}{\mathfrak{I}} \|v_h\|_{L^2(K)}^2 \le m_h^K(v_h, v_h) \le \tilde{\mathfrak{I}} \|v_h\|_{L^2(K)}^2, \quad \underset{\sim}{\xi} |v_h|_{H^1(K)}^2 \le a_h^K(v_h, v_h) \le \tilde{\xi} |v_h|_{H^1(K)}^2. \tag{2.13}$$

According to the stability and symmetry of $m_h^K(\cdot,\cdot)$ and $a_h^K(\cdot,\cdot)$, we can further derive the continuity result

$$m_h^K(u_h, v_h) \le \tilde{\mathfrak{I}} \|u_h\|_{L^2(K)} \|v_h\|_{L^2(K)}, \quad a_h(u_h, v_h) \le \tilde{\xi} |u_h|_{H^1(K)} |v_h|_{H^1(K)}. \tag{2.14}$$

The global bilinear forms $m_h(\cdot,\cdot)$ and $a_h(\cdot,\cdot)$ can be expressed as

$$m_h(u_h, v_h) = \sum_{K \in \mathcal{T}_h} m_h^K(u_h, v_h), \quad a_h(u_h, v_h) = \sum_{K \in \mathcal{T}_h} a_h^K(u_h, v_h), \quad \forall u_h, v_h \in \tilde{V}_h.$$

To derive the subsequent error estimates, we define the following norm:

$$\|v_h\|_h^2 = m_h(v_h, v_h), \quad \|\nabla v_h\|_h^2 = a_h(v_h, v_h), \quad \forall v_h \in \tilde{V}_h. \tag{2.15}$$

2.3. Fully discrete MVEM scheme

In this section, to obtain the fully discrete MVEM scheme of (2.1), we split the time interval $[0, T]$ using a uniform time grid $\mathcal{G}_{\Delta t}$ with $N + 1$ points, where $\mathcal{G}_{\Delta t} = \{t_n = n\Delta t | n = 0, 1, 2, ..., N\}$ and $\Delta t = T/N$ is the uniform time step. Let u^n be the value of $u(\cdot, t^n)$ for any smooth function u on $[0, T]$.

For the partial derivative $\frac{\partial u}{\partial t}$ at the mid-time level $t_{n-\frac{\alpha}{2}}$, the following numerical approximation can be found in [29]:

$$\frac{\partial u}{\partial t}(t_{n-\frac{\alpha}{2}}) = \begin{cases} \delta_t^\alpha u^{n-\frac{\alpha}{2}} + O(\Delta t^2), & n \geq 2, \\ \delta_t u^1 + O(\Delta t), & n = 1, \end{cases} \tag{2.16}$$

where $\delta_t^\alpha u^{n-\frac{\alpha}{2}} = \frac{(3-\alpha)u^n - (4-2\alpha)u^{n-1} + (1-\alpha)u^{n-2}}{2\Delta t}$ and $\delta_t u^1 = \frac{u^1 - u^0}{\Delta t}$.

To construct the fully discrete scheme for (2.1), we introduce two key lemmas. These lemmas provide the necessary mathematical foundation for the treatment of the fractional derivative.

Lemma 2.1. *Assuming $g \in C^2([0, T])$, we have the following second-order approximation:*

$$g\left(t_{n-\frac{\alpha}{2}}\right) = g^{n-\frac{\alpha}{2}} + O(\Delta t^2), \tag{2.17}$$

where $g^n = g(t_n)$ and the linear interpolation $g^{n-\frac{\alpha}{2}} = \left(1 - \frac{\alpha}{2}\right) g^n + \frac{\alpha}{2} g^{n-1}$.

Lemma 2.2 ([6,29,30])**.** *With $0 < \alpha < 1$ and $u \in C^3([0, T])$, the Riemann-Liouville fractional derivative can be approximated by*

$$\frac{\partial^\alpha u}{\partial t^\alpha}(t_{n-\frac{\alpha}{2}}) = \Delta t^{-\alpha} \sum_{k=0}^{n} w_k^{(\alpha)} u^{n-k} + O(\Delta t^2), \tag{2.18}$$

where $w_0^{(\alpha)} = 1$, $w_k^{(\alpha)} = (-1)^k \binom{\alpha}{k} = (1 - \frac{\alpha+1}{k}) w_{k-1}^{(\alpha)} < 0$, $k \geq 1$, where it holds that $\sum_{k=1}^{\infty} w_k^{(\alpha)} = -1$. Moreover, at time $t_{n-\frac{\alpha}{2}}$, the following relationship also holds:

$$\Delta t^{-\alpha} \sum_{k=0}^{n} w_k^{(\alpha)} v^{n-k} = \Delta t^{-\alpha} \sum_{k=0}^{n} w_k^{(\alpha)} v^{n-k-\frac{\alpha}{2}} + O(\Delta t^2). \tag{2.19}$$

Proof. The second-order approximation (2.18) can be obtained from Lemma 1 in [29], where the shifted Grünwald operator is shown to achieve $O(\Delta t^2)$ accuracy under the regularity assumption $u \in C^3([0, T])$. Furthermore, Lemma 2.4 in [6] systematizes this analysis and applies it to time discretization schemes for fractional differential equations, which yields (2.19). □

Based on the lemmas above, we get the following fully discrete MVEM scheme of (2.2): find $u_h^n, \sigma_h^n \in \tilde{V}_h(\Omega)$, such that

$$\begin{cases} m_h(\delta_t u_h^1, v_h) + \Delta t^{-\alpha} \sum\limits_{k=0}^{1} w_k^{(\alpha)} a_h(u_h^{1-k-\frac{\alpha}{2}}, v_h) + a_h(u_h^{1-\frac{\alpha}{2}}, v_h) - a_h(\sigma_h^{1-\frac{\alpha}{2}}, v_h) \\ = (f_h(u_h^{1-\frac{\alpha}{2}}), v_h) + (g_h^{1-\frac{\alpha}{2}}, v_h), \quad \forall v_h \in \tilde{V}_h(\Omega), \\ (\sigma_h^{1-\frac{\alpha}{2}}, w_h) + a_h(u_h^{1-\frac{\alpha}{2}}, w_h) = 0, \quad \forall w_h \in \tilde{V}_h(\Omega), n = 1, \end{cases} \tag{2.20}$$

when $n \geq 2$, which is to find $u_h^n, \sigma_h^n \in \tilde{V}_h(\Omega)$, such that

$$\begin{cases} m_h(\delta_t^\alpha u_h^{n-\frac{\alpha}{2}}, v_h) + \Delta t^{-\alpha} \sum_{k=0}^{n} w_k^{(\alpha)} a_h(u_h^{n-k-\frac{\alpha}{2}}, v_h) + a_h(u_h^{n-\frac{\alpha}{2}}, v_h) - a_h(\sigma_h^{n-\frac{\alpha}{2}}, v_h) \\ = (f_h(u_h^{n-\frac{\alpha}{2}}), v_h) + (g_h^{n-\frac{\alpha}{2}}, v_h), \quad \forall v_h \in \tilde{V}_h(\Omega), \\ (\sigma_h^{n-\frac{\alpha}{2}}, w_h) + a_h(u_h^{n-\frac{\alpha}{2}}, w_h) = 0, \quad \forall w_h \in \tilde{V}_h(\Omega). \end{cases} \tag{2.21}$$

For the nonlinear forcing term $f_h(u_h)$, we have

$$(f_h(u_h), v_h) = \sum_{K \in \mathcal{T}_h} \int_K f_h(u_h)\, v_h = \sum_{K \in \mathcal{T}_h} \int_K \Pi_{k,K}^0 f(\Pi_{k,K}^0 u_h)\, v_h = \sum_{K \in \mathcal{T}_h} \int_K f(\Pi_{k,K}^0 u_h)\, \Pi_{k,K}^0 v_h. \tag{2.22}$$

3. Two-grid MVEM and stability analysis

To solve the nonlinear system (2.20)–(2.21), we develop a two-grid MVEM. The approach includes two discrete levels: a coarse grid $\mathcal{T}_H$ and a fine grid $\mathcal{T}_h$, consisting of polygonal elements partitioning the domain Ω, with mesh sizes H and h satisfying $h \ll H$.

We first obtain approximate solutions u_H, σ_H in the virtual element space $\tilde{V}_H(\Omega)$ by Newton nonlinear iteration on the coarse grid $\mathcal{T}_H$. Then, based on our approximate solutions, we utilize an interpolation technique from [31] and linearize the system on the fine grid $\mathcal{T}_h$, thereby achieving more accurate solutions u_h, σ_h in the virtual element space $\tilde{V}_h(\Omega)$. The projections $\Pi_k^{0,H}$ and $\Pi_k^{0,h}$ are based on two grid partitions $\mathcal{T}_H$ and $\mathcal{T}_h$.

Our two-grid MVEM is designed as follows:

Step I: Solve the following nonlinear systems to find $\{u_H, \sigma_H\} \in \tilde{V}_H \times \tilde{V}_H$ on a coarse grid $\mathcal{T}_H$, such that for any $\{v_H, w_H\} \in \tilde{V}_H \times \tilde{V}_H$:

Case I_1: when $n = 1$,

$$\begin{cases} m_h(\delta_t u_H^1, v_H) + \Delta t^{-\alpha} \sum_{k=0}^{1} w_k^{(\alpha)} a_h(u_H^{1-k-\frac{\alpha}{2}}, v_H) + a_h(u_H^{1-\frac{\alpha}{2}}, v_H) - a_h(\sigma_H^{1-\frac{\alpha}{2}}, v_H) \\ = (\Pi_k^{0,H} f(\Pi_k^{0,H} u_H^{1-\frac{\alpha}{2}}), v_H) + (g_h^{1-\frac{\alpha}{2}}, v_H), \\ m_h(\sigma_H^{1-\frac{\alpha}{2}}, w_H) + a_h(u_H^{1-\frac{\alpha}{2}}, w_H) = 0. \end{cases} \tag{3.1}$$

Case I_2: when $n \geq 2$,

$$\begin{cases} m_h(\delta_t^\alpha u_H^{n-\frac{\alpha}{2}}, v_H) + \Delta t^{-\alpha} \sum_{k=0}^{n} w_k^{(\alpha)} a_h(u_H^{n-k-\frac{\alpha}{2}}, v_H) + a_h(u_H^{n-\frac{\alpha}{2}}, v_H) - a_h(\sigma_H^{n-\frac{\alpha}{2}}, v_H) \\ = (\Pi_k^{0,H} f(\Pi_k^{0,H} u_H^{n-\frac{\alpha}{2}}), v_H) + (g_h^{n-\frac{\alpha}{2}}, v_H), \\ m_h(\sigma_H^{n-\frac{\alpha}{2}}, w_H) + a_h(u_H^{n-\frac{\alpha}{2}}, w_H) = 0. \end{cases} \tag{3.2}$$

Step II: Solve the following linear systems to find $\{u_h, \sigma_h\} \in \tilde{V}_h \times \tilde{V}_h$ on a fine grid $\mathcal{T}_h$, such that for any $\{v_h, w_h\} \in \tilde{V}_h \times \tilde{V}_h$:

Case II_1: when $n = 1$,

$$\begin{cases} m_h(\delta_t u_h^1, v_h) + \Delta t^{-\alpha} \sum_{k=0}^{1} w_k^{(\alpha)} a_h(u_h^{1-k-\frac{\alpha}{2}}, v_h) + a_h(u_h^{1-\frac{\alpha}{2}}, v_h) - a_h(\sigma_h^{1-\frac{\alpha}{2}}, v_h) \\ = \left(\Pi_k^{0,h} f(\Pi_k^{0,H} u_H^{1-\frac{\alpha}{2}}) + \Pi_k^{0,h} f'(\Pi_k^{0,H} u_H^{1-\frac{\alpha}{2}})(\Pi_k^{0,h} u_h^{1-\frac{\alpha}{2}} - \Pi_k^{0,H} u_H^{1-\frac{\alpha}{2}}), v_h\right) + (g_h^{1-\frac{\alpha}{2}}, v_h), \\ m_h(\sigma_h^{1-\frac{\alpha}{2}}, w_h) + a_h(u_h^{1-\frac{\alpha}{2}}, w_h) = 0. \end{cases} \tag{3.3}$$

Case II_2: when $n \geq 2$,

$$\begin{cases} m_h(\delta_t^\alpha u_h^{n-\frac{\alpha}{2}}, v_h) + \Delta t^{-\alpha} \sum\limits_{k=0}^{n} w_k^{(\alpha)} a_h(u_h^{n-k-\frac{\alpha}{2}}, v_h) + a_h(u_h^{n-\frac{\alpha}{2}}, v_h) - a_h(\sigma_h^{n-\frac{\alpha}{2}}, v_h) \\ = \left(\Pi_k^{0,h} f(\Pi_k^{0,H} u_H^{n-\frac{\alpha}{2}}) + \Pi_k^{0,h} f'(\Pi_k^{0,H} u_H^{n-\frac{\alpha}{2}})(\Pi_k^{0,h} u_h^{n-\frac{\alpha}{2}} - \Pi_k^{0,H} u_H^{n-\frac{\alpha}{2}}), v_h\right) + (g_h^{n-\frac{\alpha}{2}}, v_h), \\ m_h(\sigma_h^{n-\frac{\alpha}{2}}, w_h) + a_h(u_h^{n-\frac{\alpha}{2}}, w_h) = 0. \end{cases} \tag{3.4}$$

Next, we will present some crucial lemmas that play an important role in analyzing the stability of our proposed scheme.

Lemma 3.1. *For the discrete bilinear form $m_h(\cdot,\cdot) : \tilde{V}_h \times \tilde{V}_h \mapsto \mathbb{R}$ and the norm $\|\cdot\|_h$ defined before, the sequence $\{\psi^n\}$ in the virtual element space $\tilde{V}_h$ satisfies the following relationship: for all $n \geq 2$,*

$$m_h(\delta_t^\alpha \psi^{n-\frac{\alpha}{2}}, \psi^{n-\frac{\alpha}{2}}) \geq \frac{1}{4\Delta t}(\mathscr{F}(\psi^n) - \mathscr{F}(\psi^{n-1})), \tag{3.5}$$

where $\mathscr{F}(\psi^n)$ is denoted as

$$\mathscr{F}(\psi^n) = (3-\alpha)\|\psi^n\|_h^2 - (1-\alpha)\|\psi^{n-1}\|_h^2 + (2-\frac{\alpha}{2})(1-\alpha)\|\psi^n - \psi^{n-1}\|_h^2 \geq \|\psi^n\|_h^2. \tag{3.6}$$

Proof. According to the proof techniques established in [32], we complete the proof of Lemma 3.1. □

Lemma 3.2. *For the discrete bilinear form $a_h(\cdot,\cdot) : \tilde{V}_h \times \tilde{V}_h \mapsto \mathbb{R}$ defined before, the sequence $\{\psi^n\}$ in the virtual element space $\tilde{V}_h$ satisfies the following relationship: for $m = 0, 1, \ldots, N$,*

$$\Delta t^{-\alpha} \sum_{n=0}^{m} \sum_{k=0}^{n} w_k^{(\alpha)} a_h(\psi^{n-k}, \psi^n) \geq 0. \tag{3.7}$$

Proof. We obtain the conclusion of Lemma 3.2 is a similar way as in [29]. □

3.1. Stability analysis on the coarse grid

Building upon the results provided in the preceding lemmas, we now derive the stability result of the fully discrete system on the coarse grid, as presented in Theorem 3.1.

Theorem 3.1. *For the scheme* (3.1)–(3.2) *on the coarse grid $\mathcal{T}_H$, the following stability condition holds:*

$$\|u_H^m\|^2 + \Delta t \sum_{n=1}^{m} (\|\nabla u_H^{n-\frac{\alpha}{2}}\|^2 + \|\sigma_H^{n-\frac{\alpha}{2}}\|^2) \leq C(\|u_H^0\|^2 + \Delta t \sum_{n=0}^{m} \|g^n\|^2), \quad m = 1, 2, \ldots, N. \tag{3.8}$$

Proof. According to the proof technique of Theorem 3.4 in [6], we derive a similar inequality:

$$\begin{aligned} &\|u_H^1\|_h^2 - \|u_H^0\|_h^2 + 2\Delta t^{1-\alpha} \sum_{k=0}^{1} w_k^{(\alpha)} a_h(u_H^{1-k-\frac{\alpha}{2}}, u_H^{1-\frac{\alpha}{2}}) + 2\Delta t(\|\nabla u_H^{1-\frac{\alpha}{2}}\|_h^2 + \|\sigma_H^{1-\frac{\alpha}{2}}\|_h^2) \\ &\leq 2\Delta t \|f_h(u_H^{1-\frac{\alpha}{2}})\| \|u_H^{1-\frac{\alpha}{2}}\| + \Delta t(\|u_H^{1-\frac{\alpha}{2}}\|^2 + \|g_h^{1-\frac{\alpha}{2}}\|^2). \end{aligned} \tag{3.9}$$

For the nonlinear term, by using (2.22), we get the following estimate:

$$
\begin{aligned}
\|f_h(u_H^{1-\frac{\alpha}{2}})\|^2 &= \sum_{K\in\mathcal{T}_h}\int_K |f_h(u_H^{1-\frac{\alpha}{2}})|^2 = \sum_{K\in\mathcal{T}_h}\int_K |\Pi_{k,K}^{0,H} f(\Pi_{k,K}^{0,H} u_H^{1-\frac{\alpha}{2}})|^2 \\
&= \sum_{K\in\mathcal{T}_h} \|\Pi_{k,K}^{0,H} f(\Pi_{k,K}^{0,H} u_H^{1-\frac{\alpha}{2}})\|_{0,K}^2 \leq \sum_{K\in\mathcal{T}_h} \|f(\Pi_{k,K}^{0,H} u_H^{1-\frac{\alpha}{2}})\|_{0,K}^2 \\
&\leq C_L^2 \sum_{K\in\mathcal{T}_h} \|\Pi_{k,K}^{0,H} u_H^{1-\frac{\alpha}{2}}\|_{0,K}^2 \leq C_L^2 \|u_H^{1-\frac{\alpha}{2}}\|^2.
\end{aligned}
\tag{3.10}
$$

In a similar way as in (3.10), we derive that

$$
\|g_h^{1-\frac{\alpha}{2}}\|^2 \leq 2(\|g^1\|^2 + \|g^0\|^2). \tag{3.11}
$$

Substituting (3.10) and (3.11) into (3.9), and combining the case for $n \geq 2$, we have

$$
\begin{aligned}
&\|u_H^m\|_h^2 + 4\Delta t^{1-\alpha} \sum_{n=0}^{m}\sum_{k=0}^{n} w_k^{(\alpha)} a_h(u_H^{n-k-\frac{\alpha}{2}}, u_H^{n-\frac{\alpha}{2}}) + 4\Delta t \sum_{n=1}^{m} (\|\nabla u_H^{n-\frac{\alpha}{2}}\|_h^2 + \|\sigma_H^{n-\frac{\alpha}{2}}\|_h^2) \\
&\leq C_1\|u_H^0\|_h^2 + C_2\Delta t(2C_L+1)\sum_{n=1}^{m}(\|u_H^n\|^2 + \|u_H^{n-1}\|^2) + C_3\Delta t\sum_{n=1}^{m}(\|g^n\|^2 + \|g^{n-1}\|^2).
\end{aligned}
\tag{3.12}
$$

According to the equivalence of norms $\|\cdot\|$ and $\|\cdot\|_h$, and then by using the discrete Grönwall inequality and Lemma 3.2, we finish the proof. □

3.2. *Stability analysis on the fine grid*

Based on the previous analysis on the coarse grid, we now derive the stability result on the fine grid.

Theorem 3.2. *For the scheme* (3.3)–(3.4) *on the fine grid $\mathcal{T}_h$, the following stability estimate holds:*

$$
\|u_h^m\|^2 + \Delta t\sum_{n=1}^{m}(\|\nabla u_h^{n-\frac{\alpha}{2}}\|^2 + \|\sigma_h^{n-\frac{\alpha}{2}}\|^2) \leq C(\|u_H^0\|^2 + \|u_h^0\|^2 + \Delta t\sum_{n=0}^{m}\|g^n\|^2), \quad m = 1,2,\ldots,N. \tag{3.13}
$$

Proof. Setting $v_h = u_h^{1-\frac{\alpha}{2}}$ and $w_h = \sigma_h^{1-\frac{\alpha}{2}}$ in (3.3) and summing the resulting equations, we obtain

$$
\begin{aligned}
&m_h(\delta_t u_h^1, u_h^{1-\frac{\alpha}{2}}) + \Delta t^{-\alpha}\sum_{k=0}^{1} w_k^{(\alpha)} a_h(u_h^{1-k-\frac{\alpha}{2}}, u_h^{1-\frac{\alpha}{2}}) + a_h(u_h^{1-\frac{\alpha}{2}}, u_h^{1-\frac{\alpha}{2}}) + m_h(\sigma_h^{1-\frac{\alpha}{2}}, \sigma_h^{1-\frac{\alpha}{2}}) \\
&= \Big(\Pi_k^{0,h} f(\Pi_k^{0,H} u_H^{1-\frac{\alpha}{2}}) + \Pi_k^{0,h} f'(\Pi_k^{0,H} u_H^{1-\frac{\alpha}{2}})(\Pi_k^{0,h} u_h^{1-\frac{\alpha}{2}} - \Pi_k^{0,H} u_H^{1-\frac{\alpha}{2}}), u_h^{1-\frac{\alpha}{2}}\Big) + (g_h^{1-\frac{\alpha}{2}}, u_h^{1-\frac{\alpha}{2}}).
\end{aligned}
\tag{3.14}
$$

According to the norms defined by (2.15) and (2.22), we rewrite (3.14) as

$$
\begin{aligned}
&\frac{1}{2}\delta_t\|u_h^1\|_h^2 + \frac{(1-\alpha)\Delta t}{2}\|\delta_t u_h^1\|_h^2 + \Delta t^{-\alpha}\sum_{k=0}^{1} w_k^{(\alpha)} a_h(u_h^{1-k-\frac{\alpha}{2}}, u_h^{1-\frac{\alpha}{2}}) + \|\nabla u_h^{1-\frac{\alpha}{2}}\|_h^2 + \|\sigma_h^{1-\frac{\alpha}{2}}\|_h^2 \\
&= \Big(f(\Pi_k^{0,H} u_H^{1-\frac{\alpha}{2}}) + f'(\Pi_k^{0,H} u_H^{1-\frac{\alpha}{2}})(\Pi_k^{0,h} u_h^{1-\frac{\alpha}{2}} - \Pi_k^{0,H} u_H^{1-\frac{\alpha}{2}}), \Pi_k^{0,h} u_h^{1-\frac{\alpha}{2}}\Big) + (g_h^{1-\frac{\alpha}{2}}, u_h^{1-\frac{\alpha}{2}}).
\end{aligned}
\tag{3.15}
$$

Multiplying (3.15) by $2\Delta t$, removing the positive term $\frac{(1-\alpha)\Delta t}{2}\|\delta_t u_h^1\|_h^2$, and applying the Cauchy-Schwarz inequality, Young inequality, and (2.10), we get

$$\begin{aligned}
&\|u_h^1\|_h^2 - \|u_h^0\|_h^2 + 2\Delta t^{1-\alpha}\sum_{k=0}^{1} w_k^{(\alpha)} a_h(u_h^{1-k-\frac{\alpha}{2}}, u_h^{1-\frac{\alpha}{2}}) + 2\Delta t(\|\nabla u_h^{1-\frac{\alpha}{2}}\|_h^2 + \|\sigma_h^{1-\frac{\alpha}{2}}\|_h^2) \\
&\le 2\Delta t\|f(\Pi_k^{0,H}u_H^{1-\frac{\alpha}{2}}) + f'(\Pi_k^{0,H}u_H^{1-\frac{\alpha}{2}})(\Pi_k^{0,h}u_h^{1-\frac{\alpha}{2}} - \Pi_k^{0,H}u_H^{1-\frac{\alpha}{2}})\|\|u_h^{1-\frac{\alpha}{2}}\| \\
&\quad + \Delta t(\|u_h^{1-\frac{\alpha}{2}}\|^2 + \|g_h^{1-\frac{\alpha}{2}}\|^2).
\end{aligned} \tag{3.16}$$

According to (2.22), we have the following estimation:

$$\begin{aligned}
&\|f(\Pi_k^{0,H}u_H^{1-\frac{\alpha}{2}}) + f'(\Pi_k^{0,H}u_H^{1-\frac{\alpha}{2}})(\Pi_k^{0,h}u_h^{1-\frac{\alpha}{2}} - \Pi_k^{0,H}u_H^{1-\frac{\alpha}{2}})\| \\
&\le \|f(\Pi_k^{0,H}u_H^{1-\frac{\alpha}{2}})\| + \|f'(\Pi_k^{0,H}u_H^{1-\frac{\alpha}{2}})\|_{0,\infty}(\|\Pi_k^{0,h}u_h^{1-\frac{\alpha}{2}}\| + \|\Pi_k^{0,H}u_H^{1-\frac{\alpha}{2}}\|) \\
&\le C_L\|u_H^{1-\frac{\alpha}{2}}\| + \|f'(\Pi_k^{0,H}u_H^{1-\frac{\alpha}{2}})\|_{0,\infty}(\|u_h^{1-\frac{\alpha}{2}}\| + \|u_H^{1-\frac{\alpha}{2}}\|),
\end{aligned} \tag{3.17}$$

where $\|f'(\Pi_k^{0,H}u_H^{1-\frac{\alpha}{2}})\|_{0,\infty} \le M$. Substituting (3.17) and (3.11) into (3.9), we get

$$\begin{aligned}
&\|u_h^1\|_h^2 - \|u_h^0\|_h^2 + 2\Delta t^{1-\alpha}\sum_{k=0}^{1} w_k^{(\alpha)} a_h(u_h^{1-k-\frac{\alpha}{2}}, u_h^{1-\frac{\alpha}{2}}) + 2\Delta t(\|\nabla u_h^{1-\frac{\alpha}{2}}\|_h^2 + \|\sigma_h^{1-\frac{\alpha}{2}}\|_h^2) \\
&\le 2\Delta t(C_L + M)(\|u_H^1\|^2 + \|u_H^0\|^2) + 4\Delta t(M+1)(\|u_h^1\|^2 + \|u_h^0\|^2) + 2\Delta t(\|g_h^1\|^2 + \|g_h^0\|^2).
\end{aligned} \tag{3.18}$$

Setting $v_h = u_h^{n-\frac{\alpha}{2}}$ and $w_h = \sigma_h^{n-\frac{\alpha}{2}}$ in (3.4), for $n \ge 2$, we get

$$\begin{aligned}
&m_h(\delta_t^\alpha u_h^{n-\frac{\alpha}{2}}, u_h^{n-\frac{\alpha}{2}}) + \Delta t^{-\alpha}\sum_{k=0}^{n} w_k^{(\alpha)} a_h(u_h^{n-k-\frac{\alpha}{2}}, u_h^{n-\frac{\alpha}{2}}) + a_h(u_h^{n-\frac{\alpha}{2}}, u_h^{n-\frac{\alpha}{2}}) + m_h(\sigma_h^{n-\frac{\alpha}{2}}, \sigma_h^{n-\frac{\alpha}{2}}) \\
= &\left(\Pi_k^{0,h}f(\Pi_k^{0,H}u_H^{n-\frac{\alpha}{2}}) + \Pi_k^{0,h}f'(\Pi_k^{0,H}u_H^{n-\frac{\alpha}{2}})(\Pi_k^{0,h}u_h^{n-\frac{\alpha}{2}} - \Pi_k^{0,H}u_H^{n-\frac{\alpha}{2}}), u_h^{n-\frac{\alpha}{2}}\right) + (g_h^{n-\frac{\alpha}{2}}, u_h^{n-\frac{\alpha}{2}}).
\end{aligned} \tag{3.19}$$

Using the Cauchy-Schwarz inequality and Lemma 3.1, and summing (3.19) from $n = 2$ to m, we obtain

$$\begin{aligned}
&\frac{\mathscr{F}(u_h^m) - \mathscr{F}(u_h^1)}{4\Delta t} + \Delta t^{-\alpha}\sum_{n=2}^{m}\sum_{k=0}^{n} w_k^{(\alpha)} a_h(u_h^{n-k-\frac{\alpha}{2}}, u_h^{n-\frac{\alpha}{2}}) + \sum_{n=2}^{m}(\|\nabla u_h^{n-\frac{\alpha}{2}}\|_h^2 + \|\sigma_h^{n-\frac{\alpha}{2}}\|_h^2) \\
&\le \sum_{n=2}^{m}((C_L + M)\|u_H^{n-\frac{\alpha}{2}}\| + M\|u_h^{n-\frac{\alpha}{2}}\| + \|g_h^{n-\frac{\alpha}{2}}\|)\|u_h^{n-\frac{\alpha}{2}}\|.
\end{aligned} \tag{3.20}$$

Multiplying (3.20) by $4\Delta t$ and using the Young inequality and (3.11), we get

$$\begin{aligned}
&\|u_h^m\|_h^2 + 4\Delta t^{1-\alpha}\sum_{n=2}^{m}\sum_{k=0}^{n} w_k^{(\alpha)} a_h(u_h^{n-k-\frac{\alpha}{2}}, u_h^{n-\frac{\alpha}{2}}) + 4\Delta t\sum_{n=2}^{m}(\|\nabla u_h^{n-\frac{\alpha}{2}}\|_h^2 + \|\sigma_h^{n-\frac{\alpha}{2}}\|_h^2) \\
&\le (3-\alpha)\|u_h^1\|_h^2 + (4-\alpha)(1-\alpha)(\|u_h^1\|_h^2 + \|u_h^0\|_h^2) + 4\Delta t(C_L + M)\sum_{n=2}^{m}(\|u_H^n\|^2 + \|u_H^{n-1}\|^2) \\
&\quad + 8\Delta t(M+1)\sum_{n=2}^{m}(\|u_h^n\|^2 + \|u_h^{n-1}\|^2) + 4\Delta t\sum_{n=2}^{m}(\|g^n\|^2 + \|g^{n-1}\|^2).
\end{aligned} \tag{3.21}$$

Combining (3.18) with (3.21), and leveraging the norm equivalence between $\|\cdot\|$ and $\|\cdot\|_h$, we obtain

$$\begin{aligned}&\|u_h^m\|^2+4\Delta t^{1-\alpha}\sum_{n=0}^{m}\sum_{k=0}^{n}w_k^{(\alpha)}a_h(u_h^{n-k-\frac{\alpha}{2}},u_h^{n-\frac{\alpha}{2}})+4\Delta t\sum_{n=1}^{m}(\|\nabla u_H^{n-\frac{\alpha}{2}}\|^2+\|\sigma_H^{n-\frac{\alpha}{2}}\|^2)\\ \le\ &C_1^*\|u_h^0\|^2+C_2^*\Delta t\sum_{n=1}^{m}(\|u_H^n\|^2+\|u_H^{n-1}\|^2)+C_3^*\Delta t\sum_{n=1}^{m}(\|g^n\|^2+\|g^{n-1}\|^2)\\ &+C_4\Delta t\sum_{n=1}^{m}(\|u_h^n\|^2+\|u_h^{n-1}\|^2).\end{aligned}\tag{3.22}$$

By Theorem 3.1, and using the discrete Grönwall inequality and Lemma 3.2, we complete the proof. □

4. A priori error analysis for the two-grid MVEM scheme

In this section, we will derive an a priori error convergence result for our proposed two-grid MVEM scheme (3.1)–(3.4). For the theoretical analysis, we assume that the domain Ω is convex, the initial data $u_0\in H^{k+1}(\Omega)$ is compatible with the boundary conditions, the nonlinear source term $f(u)$ is locally Lipschitz continuous and satisfies $|f(u)|+|f'(u)|+|f''(u)|\le M$, and the forcing term $g(x,t)$ is sufficiently smooth in time. Since the time-fractional derivative is taken in the Riemann-Liouville sense, the exact solution may in general exhibit weak singular behavior near $t=0^+$. However, when the initial data and the source term satisfy appropriate high-order compatibility conditions, the solution is assumed to satisfy the following regularity estimate, which will serve as a crucial assumption in our error analysis.

$$\|u\|_{H^{k+1}(\Omega)}+\|\sigma\|_{H^{k+1}(\Omega)}+\|u_t\|_{L^1(0,T;H^{k+1}(\Omega))}+\|u_{tt}\|_{L^1(0,T;L^2(\Omega))}+\|u_{ttt}\|_{L^1(0,T;L^2(\Omega))}\le C_r.\tag{4.1}$$

Following [17], we define the energy projection operator $\mathcal{P}^h: H_0^1(\Omega)\mapsto\tilde{V}_h$ as

$$\begin{cases}\mathcal{P}^h u\in\tilde{V}_h\\ a_h\left(\mathcal{P}^h u,v_h\right)=a\left(u,v_h\right),\forall v_h\in\tilde{V}_h.\end{cases}\tag{4.2}$$

Lemma 4.1 ([17]). *Let $u\in H_0^1(\Omega)\cap H^{k+1}(\Omega)$, and if the domain Ω is convex, there exists a unique function $\mathcal{P}^h u\in\tilde{V}_h$ satisfying*

$$\left\|\mathcal{P}^h u-u\right\|+h\left|\mathcal{P}^h u-u\right|_1\le Ch^{k+1}|u|_{k+1},\tag{4.3}$$

where C is a constant independent of h, which depends only on $\underset{\sim}{\xi}$ and $\tilde{\xi}$.

4.1. The error estimate on the coarse grid

Theorem 4.1. *Suppose that (u_H^n,σ_H^n) is the solution of discrete system* (3.1)–(3.2) *on the coarse grid. Then, there exists sufficiently small time step Δt and the spatial mesh parameter H, such that for all $m=1,2,\ldots,N$,*

$$\begin{aligned}&\|u_H^m-u^m\|+\left(\Delta t\sum_{n=1}^{m}\|\nabla u_H^{n-\frac{\alpha}{2}}-\nabla u^{n-\frac{\alpha}{2}}\|^2\right)^{\frac12}+\left(\Delta t\sum_{n=1}^{m}\|\sigma_H^{n-\frac{\alpha}{2}}-\sigma^{n-\frac{\alpha}{2}}\|^2\right)^{\frac12}\\ &\le C(\Delta t^2+H^{k+1}),\end{aligned}\tag{4.4}$$

where $C=\max\left\{C_rT,K_0T+C_{\tilde{\mathfrak{J}}^*}T|\sigma^{n-\frac{\alpha}{2}}|_{k+1}\right\}$ independent of Δt and H.

Proof. Using the energy projection operator $\mathcal{P}^h$ defined in (4.2), we split errors as follows:

$$\begin{aligned}\|u_H^n - u^n\| &\le \|u_H^n - P^h u^n\| + \|\mathcal{P}^h u^n - u^n\| := \|\wp_u^n\| + \|\eta_u^n\|,\\ \|\sigma_H^n - \sigma^n\| &\le \|\sigma_H^n - \mathcal{P}^h \sigma^n\| + \|\mathcal{P}^h \sigma^n - \sigma^n\| := \|\varsigma_\sigma^n\| + \|\varrho_\sigma^n\|.\end{aligned} \tag{4.5}$$

By the approximation properties of the projection operator $\mathcal{P}^h$ given by Lemma 4.1, we bound the projection errors:

$$\|\eta_u^n\| \le CH^{k+1}|u^n|_{k+1}, \quad \|\varrho_\sigma^n\| \le CH^{k+1}|\sigma^n|_{k+1}. \tag{4.6}$$

According to the fully discrete scheme (3.2), we derive the following error equations, for $\forall v_h, w_h \in \tilde{V}_H$:

$$\begin{aligned}&m_h(\delta_t^\alpha \wp_u^{n-\frac{\alpha}{2}}, v_H) + \Delta t^{-\alpha}\sum_{k=0}^{n} w_k^{(\alpha)} a_h(\wp_u^{n-k-\frac{\alpha}{2}}, v_H) + a_h(\wp_u^{n-\frac{\alpha}{2}}, v_H) - a_h(\varsigma_\sigma^{n-\frac{\alpha}{2}}, v_H)\\ =\ &\left(\Pi_k^{0,H} f(\Pi_k^{0,H} u_H^{n-\frac{\alpha}{2}}), v_H\right) + (g_h^{n-\frac{\alpha}{2}}, v_H) + (u_t^{n-\frac{\alpha}{2}}, v_H) - m_h(\delta_t^\alpha \mathcal{P}^h u^{n-\frac{\alpha}{2}}, v_H)\\ &- (f(u^{n-\frac{\alpha}{2}}), v_H) - (g^{n-\frac{\alpha}{2}}, v_H),\end{aligned} \tag{4.7}$$

$$m_h(\varsigma_\sigma^{n-\frac{\alpha}{2}}, w_h) + a_h(\wp_u^{n-\frac{\alpha}{2}}, w_h) = (\sigma^{n-\frac{\alpha}{2}}, w_h) - m_h(\mathcal{P}^h \sigma^{n-\frac{\alpha}{2}}, w_h). \tag{4.8}$$

Substituting $v_H = \wp_u^{n-\frac{\alpha}{2}}$ into (4.7) and $w_h = \varsigma_\sigma^{n-\frac{\alpha}{2}}$ into (4.8), and summing the two equations, yields

$$\begin{aligned}&m_h(\delta_t^\alpha \wp_u^{n-\frac{\alpha}{2}}, \wp_u^{n-\frac{\alpha}{2}}) + \Delta t^{-\alpha}\sum_{k=0}^{n} w_k^{(\alpha)} a_h(\wp_u^{n-k-\frac{\alpha}{2}}, \wp_u^{n-\frac{\alpha}{2}}) + a_h(\wp_u^{n-\frac{\alpha}{2}}, \wp_u^{n-\frac{\alpha}{2}}) + m_h(\varsigma_\sigma^{n-\frac{\alpha}{2}}, \varsigma_\sigma^{n-\frac{\alpha}{2}})\\ =\ &(\Pi_k^{0,H} f(\Pi_k^{0,H} u_H^{n-\frac{\alpha}{2}}), \wp_u^{n-\frac{\alpha}{2}}) + (g_h^{n-\frac{\alpha}{2}}, \wp_u^{n-\frac{\alpha}{2}}) + (u_t^{n-\frac{\alpha}{2}}, \wp_u^{n-\frac{\alpha}{2}}) - m_h(\delta_t^\alpha \mathcal{P}^h u^{n-\frac{\alpha}{2}}, \wp_u^{n-\frac{\alpha}{2}})\\ &- (f(u^{n-\frac{\alpha}{2}}), \wp_u^{n-\frac{\alpha}{2}}) - (g^{n-\frac{\alpha}{2}}, \wp_u^{n-\frac{\alpha}{2}}) + (\sigma^{n-\frac{\alpha}{2}}, \varsigma_\sigma^{n-\frac{\alpha}{2}}) - m_h(\mathcal{P}^h \sigma^{n-\frac{\alpha}{2}}, \varsigma_\sigma^{n-\frac{\alpha}{2}})\\ :=\ &\mathscr{A}_1^n + \mathscr{A}_2^n + \mathscr{A}_3^n + \mathscr{A}_4^n.\end{aligned} \tag{4.9}$$

In order to estimate the first term $\mathscr{A}_1^n$ on the right-hand side of (4.9), by using (2.22), we have

$$\begin{aligned}|\mathscr{A}_1^n| &= |(\Pi_k^{0,H} f(\Pi_k^{0,H} u_H^{n-\frac{\alpha}{2}}), \wp_u^{n-\frac{\alpha}{2}}) - (f(u^{n-\frac{\alpha}{2}}), \wp_u^{n-\frac{\alpha}{2}})|\\ &\le \sum_{K\in\mathcal{T}_h} |(f(\Pi_{k,K}^{0,H} u_H^{n-\frac{\alpha}{2}}) - f(\Pi_{k,K}^{0,H} u^{n-\frac{\alpha}{2}}), \Pi_{k,K}^{0,H} \wp_u^{n-\frac{\alpha}{2}})_K\\ &\quad + (f(\Pi_{k,K}^{0,H} u^{n-\frac{\alpha}{2}}) - f(u^{n-\frac{\alpha}{2}}), \Pi_{k,K}^{0,H} \wp_u^{n-\frac{\alpha}{2}})_K\\ &\quad + (\Pi_{k,K}^{0,H} f(u^{n-\frac{\alpha}{2}}) - f(u^{n-\frac{\alpha}{2}}), \wp_u^{n-\frac{\alpha}{2}})_K|.\end{aligned} \tag{4.10}$$

Then by applying the Cauchy-Schwarz inequality, (2.10), and (2.11), we obtain

$$\begin{aligned}|\mathscr{A}_1^n| &\le (C_L\|\Pi_{k,K}^{0,H} u_H^{n-\frac{\alpha}{2}} - \Pi_{k,K}^{0,H} u^{n-\frac{\alpha}{2}}\| + C_L\|\Pi_{k,K}^{0,H} u^{n-\frac{\alpha}{2}} - u^{n-\frac{\alpha}{2}}\|\\ &\quad + \|\Pi_{k,K}^{0,H} f(u^{n-\frac{\alpha}{2}}) - f(u^{n-\frac{\alpha}{2}})\|)\|\wp_u^{n-\frac{\alpha}{2}}\|\\ &\le (C_L(\|\wp_u^{n-\frac{\alpha}{2}}\| + \|\eta_u^{n-\frac{\alpha}{2}}\|) + C_\pi H^{k+1}(|u^{n-\frac{\alpha}{2}}|_{k+1} + |f(u^{n-\frac{\alpha}{2}})|_{k+1}))\|\wp_u^{n-\frac{\alpha}{2}}\|.\end{aligned} \tag{4.11}$$

For the second term $\mathscr{A}_2^n$, similar to the estimation process above, we get

$$\begin{aligned}|\mathscr{A}_2^n| &= |(g_h^{n-\frac{\alpha}{2}}, \wp_u^{n-\frac{\alpha}{2}}) - (g^{n-\frac{\alpha}{2}}, \wp_u^{n-\frac{\alpha}{2}})|\\ &\le \sum_{K\in\mathcal{T}_h} \|\Pi_{k,K}^{0,H} g^{n-\frac{\alpha}{2}} - g^{n-\frac{\alpha}{2}}\|\|\wp_u^{n-\frac{\alpha}{2}}\|\\ &\le C_\pi H^{k+1}|g^{n-\frac{\alpha}{2}}|_{k+1}\|\wp_u^{n-\frac{\alpha}{2}}\|.\end{aligned} \tag{4.12}$$

To bound $\mathscr{A}_3^n$, we apply Lemma 4.1 alongside the consistency and the continuity of the bilinear form $m_h(\cdot,\cdot)$. By adding and subtracting suitable terms, we derive

$$
\begin{aligned}
|\mathscr{A}_3^n| &= |(u_t^{n-\frac{\alpha}{2}}, \wp_u^{n-\frac{\alpha}{2}}) - m_h(\delta_t^\alpha \mathcal{P}^h u^{n-\frac{\alpha}{2}}, \wp_u^{n-\frac{\alpha}{2}})| \\
&= |\sum_{K\in\mathcal{T}_h} ((u_t^{n-\frac{\alpha}{2}} - \delta_t^\alpha u^{n-\frac{\alpha}{2}}, \wp_u^{n-\frac{\alpha}{2}})_K + (\delta_t^\alpha u^{n-\frac{\alpha}{2}} - \Pi_{k,K}^{0,H}\delta_t^\alpha u^{n-\frac{\alpha}{2}}, \wp_u^{n-\frac{\alpha}{2}})_K \\
&\quad + m_h^K(\Pi_{k,K}^{0,H}\delta_t^\alpha u^{n-\frac{\alpha}{2}} - \mathcal{P}^h\delta_t^\alpha u^{n-\frac{\alpha}{2}}, \wp_u^{n-\frac{\alpha}{2}}))| \\
&\le \frac{C}{2\Delta t}(\|2\Delta t u_t^{n-\frac{\alpha}{2}} - ((3-\alpha)u^n - (4-2\alpha)u^{n-1} + (1-\alpha)u^{n-2})\| \\
&\quad + H^{k+1}|(3-\alpha)u^n - (4-2\alpha)u^{n-1} + (1-\alpha)u^{n-2}|_{k+1})\|\wp_u^{n-\frac{\alpha}{2}}\| \\
&\le \frac{C}{2\Delta t}(\|2\Delta t(u_t(t_{n-\frac{\alpha}{2}}) + O(\Delta t^2)) - ((3-\alpha)u^n - (4-2\alpha)u^{n-1} + (1-\alpha)u^{n-2})\| \\
&\quad + H^{k+1}|(3-\alpha)\int_{t_{n-1}}^{t_n} u_t(t)dt - (1-\alpha)\int_{t_{n-2}}^{t_{n-1}} u_t(t)dt|_{k+1})\|\wp_u^{n-\frac{\alpha}{2}}\| \\
&\le C(\Delta t^2\|u_{ttt}\|_{L^1(0,t_n,L^2(\Omega))} + H^{k+1}\|u_t\|_{L^1(0,t_n,H^{k+1}(\Omega))})\|\wp_u^{n-\frac{\alpha}{2}}\|.
\end{aligned} \tag{4.13}
$$

In the same way, for $\mathscr{A}_4^n$, we have

$$
\begin{aligned}
|\mathscr{A}_4^n| &= |(\sigma^{n-\frac{\alpha}{2}}, \varsigma_\sigma^{n-\frac{\alpha}{2}}) - m_h(\mathcal{P}^h\sigma^{n-\frac{\alpha}{2}}, \varsigma_\sigma^{n-\frac{\alpha}{2}})| \\
&= |\sum_{K\in\mathcal{T}_h} ((\sigma^{n-\frac{\alpha}{2}} - \Pi_{k,K}^{0,H}\sigma^{n-\frac{\alpha}{2}}, \varsigma_\sigma^{n-\frac{\alpha}{2}})_K - m_h^K(\mathcal{P}^h\sigma^{n-\frac{\alpha}{2}} - \Pi_{k,K}^{0,H}\sigma^{n-\frac{\alpha}{2}}, \varsigma_\sigma^{n-\frac{\alpha}{2}}))| \\
&\le \max(1,\tilde{\mathfrak{J}})\sum_{K\in\mathcal{T}_h}(\|\sigma^{n-\frac{\alpha}{2}} - \Pi_{k,K}^{0,H}\sigma^{n-\frac{\alpha}{2}}\|_{0,K} + \|\mathcal{P}^h\sigma^{n-\frac{\alpha}{2}} - \Pi_{k,K}^{0,H}\sigma^{n-\frac{\alpha}{2}}\|_{0,K})\|\varsigma_\sigma^{n-\frac{\alpha}{2}}\| \\
&\le C_{\tilde{\mathfrak{J}}^*}H^{k+1}|\sigma^{n-\frac{\alpha}{2}}|_{k+1}\|\varsigma_\sigma^{n-\frac{\alpha}{2}}\|.
\end{aligned} \tag{4.14}
$$

Using Lemma 3.1, (2.15), (4.11)–(4.14), and (4.9), we get

$$
\begin{aligned}
&\frac{\mathscr{F}(\wp_u^n) - \mathscr{F}(\wp_u^{n-1})}{4\Delta t} + \Delta t^{-\alpha}\sum_{k=0}^n w_k^{(\alpha)} a_h(\wp_u^{n-k-\frac{\alpha}{2}}, \wp_u^{n-\frac{\alpha}{2}}) + \|\nabla\wp_u^{n-\frac{\alpha}{2}}\|_h^2 + \|\varsigma_\sigma^{n-\frac{\alpha}{2}}\|_h^2 \\
&\le C(\|\wp_u^{n-\frac{\alpha}{2}}\| + \|\eta_u^{n-\frac{\alpha}{2}}\| + \Delta t^2\|u_{ttt}\|_{L^1(0,t_n,L^2(\Omega))} + H^{k+1}(|u^{n-\frac{\alpha}{2}}|_{k+1} + |f(u^{n-\frac{\alpha}{2}})|_{k+1} \\
&\quad + |g^{n-\frac{\alpha}{2}}|_{k+1} + \|u_t\|_{L^1(0,t_n,H^{k+1}(\Omega))}))\|\wp_u^{n-\frac{\alpha}{2}}\| + C_{\tilde{\mathfrak{J}}^*}H^{k+1}|\sigma^{n-\frac{\alpha}{2}}|_{k+1}\|\varsigma_\sigma^{n-\frac{\alpha}{2}}\|.
\end{aligned} \tag{4.15}
$$

Under the regularity assumption (4.1), we define

$$
K_0 := \max_{0\le n\le m}(|u^{n-\frac{\alpha}{2}}|_{k+1} + |f(u^{n-\frac{\alpha}{2}})|_{k+1} + |g^{n-\frac{\alpha}{2}}|_{k+1} + \|u_t\|_{L^1(0,t_n,H^{k+1}(\Omega))}). \tag{4.16}
$$

Summing (4.15) from $n = 2$ to m and substituting (4.6) into (4.15), we have

$$
\begin{aligned}
&\frac{\mathscr{F}(\wp_u^m) - \mathscr{F}(\wp_u^1)}{4\Delta t} + \Delta t^{-\alpha}\sum_{n=2}^m\sum_{k=0}^n w_k^{(\alpha)} a_h(\wp_u^{n-k-\frac{\alpha}{2}}, \wp_u^{n-\frac{\alpha}{2}}) + \sum_{n=2}^m(\|\nabla\wp_u^{n-\frac{\alpha}{2}}\|_h^2 + \|\varsigma_\sigma^{n-\frac{\alpha}{2}}\|_h^2) \\
&\le C\sum_{n=2}^m(\|\wp_u^{n-\frac{\alpha}{2}}\| + \Delta t^2\|u_{ttt}\|_{L^1(0,t_n,L^2(\Omega))} + K_0H^{k+1})\|\wp_u^{n-\frac{\alpha}{2}}\| + \sum_{n=2}^m C_{\tilde{\mathfrak{J}}^*}H^{k+1}|\sigma^{n-\frac{\alpha}{2}}|_{k+1}\|\varsigma_\sigma^{n-\frac{\alpha}{2}}\|.
\end{aligned} \tag{4.17}
$$

Furthermore, multiplying (4.17) by $4\Delta t$, we obtain

$$\begin{aligned}
&\|\wp_u^m\|_h^2 + 4\Delta t^{1-\alpha}\sum_{n=2}^{m}\sum_{k=0}^{n} w_k^{(\alpha)} a_h(\wp_u^{n-k-\frac{\alpha}{2}}, \wp_u^{n-\frac{\alpha}{2}}) + 4\Delta t\sum_{n=2}^{m}(\|\nabla\wp_u^{n-\frac{\alpha}{2}}\|_h^2 + \|\varsigma_\sigma^{n-\frac{\alpha}{2}}\|_h^2) \\
&\le 7\|\wp_u^1\|_h^2 + 4\|\wp_u^0\|_h^2 + C\Delta t\sum_{n=2}^{m}(\|\wp_u^{n-\frac{\alpha}{2}}\| + \Delta t^2\|u_{ttt}\|_{L^1(0,t_n,L^2(\Omega))} + K_0H^{k+1})\|\wp_u^{n-\frac{\alpha}{2}}\| \\
&\quad + \sum_{n=2}^{m} C_{\mathfrak{J}^*}H^{k+1}|\sigma^{n-\frac{\alpha}{2}}|_{k+1}\|\varsigma_\sigma^{n-\frac{\alpha}{2}}\|.
\end{aligned} \tag{4.18}$$

For $n = 1$, similar as with $n \ge 2$, we can obtain the following inequality:

$$\begin{aligned}
&\|\wp_u^1\|_h^2 - \|\wp_u^0\|_h^2 + 2\Delta t^{1-\alpha}\sum_{k=0}^{1} w_k^{(\alpha)} a_h(\wp_u^{1-k-\frac{\alpha}{2}}, \wp_u^{1-\frac{\alpha}{2}}) + 2\Delta t(\|\nabla\wp_u^{1-\frac{\alpha}{2}}\|_h^2 + \|\varsigma_\sigma^{1-\frac{\alpha}{2}}\|_h^2) \\
&\le C\Delta t(\|\wp_u^{1-\frac{\alpha}{2}}\| + \Delta t\|u_{tt}\|_{L^1(0,t_1,L^2(\Omega))} + K_0H^{k+1})\|\wp_u^{1-\frac{\alpha}{2}}\| \\
&\quad + 2\Delta t C_{\mathfrak{J}^*}H^{k+1}|\sigma^{1-\frac{\alpha}{2}}|_{k+1}\|\varsigma_\sigma^{1-\frac{\alpha}{2}}\|.
\end{aligned} \tag{4.19}$$

By combining (4.18) with (4.19), and using the Young inequality and regularity assumption (4.1), we obtain

$$\begin{aligned}
&\|\wp_u^m\|_h^2 + 4\Delta t^{1-\alpha}\sum_{n=1}^{m}\sum_{k=0}^{n} w_k^{(\alpha)} a_h(\wp_u^{n-k-\frac{\alpha}{2}}, \wp_u^{n-\frac{\alpha}{2}}) + 4\Delta t\sum_{n=1}^{m}(\|\nabla\wp_u^{n-\frac{\alpha}{2}}\|_h^2 + \|\varsigma_\sigma^{n-\frac{\alpha}{2}}\|_h^2) \\
&\le C\|\wp_u^0\|_h^2 + C_1\Delta t\sum_{n=1}^{m}\|\wp_u^{n-\frac{\alpha}{2}}\|^2 + \Delta t\sum_{n=1}^{m}(C_r\Delta t^2 + H^{k+1}(K_0 + C_{\mathfrak{J}^*}|\sigma^{n-\frac{\alpha}{2}}|_{k+1}))^2 \\
&\quad + 2\Delta t\sum_{n=1}^{m}\|\varsigma_\sigma^{n-\frac{\alpha}{2}}\|^2.
\end{aligned} \tag{4.20}$$

According to the norm equivalence between $\|\cdot\|$ and $\|\cdot\|_h$, we use the discrete Grönwall inequality, Lemma 3.2, and the relationship $m\Delta t \le T$ to get

$$\begin{aligned}
&\|\wp_u^m\| + \Big(\Delta t\sum_{n=1}^{m}(\|\nabla\wp_u^{n-\frac{\alpha}{2}}\|_h^2)\Big)^{\frac{1}{2}} + \Big(\Delta t\sum_{n=1}^{m}(\|\varsigma_\sigma^{n-\frac{\alpha}{2}}\|_h^2)\Big)^{\frac{1}{2}} \\
&\le C\|\wp_u^0\| + T(C_r\Delta t^2 + H^{k+1}(K_0 + C_{\mathfrak{J}^*}|\sigma^{n-\frac{\alpha}{2}}|_{k+1})).
\end{aligned} \tag{4.21}$$

Finally, by virtue of (4.5), (4.6), and $u(\cdot, 0) = u_H^0$, we complete the proof. □

4.2. The error estimate on the fine grid

Lemma 4.2 ([28,33,34]). *Let $\Omega \subset \mathbb{R}^2$ be a bounded domain with a Lipschitz boundary. Then for any $u \in H_0^1(\Omega)$, there exists a constant $C > 0$ depending only on Ω such that*

$$\|u\|_{0,4} \le C\|u\|^{\frac{1}{2}}\|\nabla u\|^{\frac{1}{2}}. \tag{4.22}$$

Lemma 4.3 ([14]). *There exists a constant C, depending only on k and ρ, such that for $u \in H^{k+1}(K)$, there exists $u_\pi \in P_k(K)$ such that*

$$\|u - u_\pi\|_{0,K} + h_K|u - u_\pi|_{1,K} \le Ch_K^{k+1}|u|_{k+1,K}. \tag{4.23}$$

Lemma 4.4. *For any $u \in W^{k+1,4}(K)$, there exists a constant C, depending only on k and the shape regularity parameter ρ of K, such that*

$$\|u - \Pi^0_{k,K}u\|_{L^4(K)} \leq Ch_K^{k+1}|u|_{W^{k+1,4}(K)}, \tag{4.24}$$

where $\Pi^0_{k,K}u \in P_k(K)$ is the local L^2-projection of u onto $P_k(K)$.

Proof. According to the classical Scott–Dupont theory (see, e.g., [35]), for any $u \in W^{k+1,p}(K)$, there exists $u_\pi \in P_k(K)$ and $u_\pi \neq \Pi^0_{k,K}u$ such that

$$\|u - u_\pi\|_{L^4(K)} \leq Ch_K^{k+1}|u|_{W^{k+1,4}(K)}. \tag{4.25}$$

By applying the triangle inequality, we decompose the error as

$$\|u - \Pi^0_{k,K}u\|_{L^4(K)} \leq \|u - u_\pi\|_{L^4(K)} + \|u_\pi - \Pi^0_{k,K}u\|_{L^4(K)}. \tag{4.26}$$

Due to $\Pi^0_{k,K}u_\pi = u_\pi$, we have

$$\|u_\pi - \Pi^0_{k,K}u\|_{L^4(K)} = \|\Pi^0_{k,K}(u - u_\pi)\|_{L^4(K)}. \tag{4.27}$$

As $\Pi^0_{k,K}$ satisfies (2.10) in the L^2-norm, according to Lemma 4.3, we obtain

$$\|\Pi^0_{k,K}(u - u_\pi)\|_{L^2(K)} \leq \|u - u_\pi\|_{L^2(K)} \leq Ch_K^{k+1}|u|_{W^{k+1,2}(K)}. \tag{4.28}$$

According to $|K| \sim h_K^d (d = 2, 3)$ and using the Hölder inequality, we derive

$$|u|_{W^{k+1,2}(K)} \leq Ch_K^{d\left(\frac{1}{2}-\frac{1}{4}\right)}|u|_{W^{k+1,4}(K)}. \tag{4.29}$$

Furthermore,

$$\|\Pi^0_{k,K}(u - u_\pi)\|_{L^2(K)} \leq Ch_K^{k+1+d\left(\frac{1}{2}-\frac{1}{4}\right)}|u|_{W^{k+1,4}(K)}. \tag{4.30}$$

For the finite-dimensional space $P_k(K)$, we have the following inverse estimate:

$$\|\Pi^0_{k,K}(u - u_\pi)\|_{L^4(K)} \leq Ch_K^{-d\left(\frac{1}{2}-\frac{1}{4}\right)}\|\Pi^0_{k,K}(u - u_\pi)\|_{L^2(K)}. \tag{4.31}$$

Combining (4.27), (4.30) with (4.31), we obtain

$$\|u_\pi - \Pi^0_{k,K}u\|_{L^4(K)} \leq Ch_K^{-d\left(\frac{1}{2}-\frac{1}{4}\right)}h_K^{k+1+d\left(\frac{1}{2}-\frac{1}{4}\right)}|u|_{W^{k+1,4}(K)} = Ch_K^{k+1}|u|_{W^{k+1,4}(K)}. \tag{4.32}$$

Then, substituting (4.25) and (4.32) into (4.26), we complete the proof. □

Building on the lemmas above, we next leverage these estimates to derive a global convergence result for the two-grid MVEM.

Theorem 4.2. *Assume that (u_h^n, σ_h^n) is the solution of the fully discrete two-grid MVEM system* (3.3)–(3.4)*, and the coarse and fine mesh sizes H and h satisfy the scaling condition $H = O(h^{1/2})$. There exists sufficiently small space mesh parameters h, H and time length size Δt, such that for all $m = 1, 2, \ldots, N$,*

$$\|u_h^m - u^m\| + \Big(\Delta t\sum_{n=1}^{m}\big(\|\nabla u_h^{n-\frac{\alpha}{2}} - \nabla u^{n-\frac{\alpha}{2}}\|^2 + \|\sigma_h^{n-\frac{\alpha}{2}} - \sigma^{n-\frac{\alpha}{2}}\|^2\big)\Big)^{\frac{1}{2}} \leq C(\Delta t^2 + h^{k+1} + H^{2k+2}), \tag{4.33}$$

where C is independent of Δt, h, and H, which depends on K_0, $C_{\mathfrak{J}^*}$, and C_r.

Proof. To bound the total errors, we apply the triangle inequality and decompose them as follows:

$$\begin{aligned} \|u_h^n - u^n\| &\le \|u_h^n - \mathcal{P}^h u^n\| + \|\mathcal{P}^h u^n - u^n\| := \|\vartheta_u^n\| + \|\varrho_u^n\|, \\ \|\sigma_h^n - \sigma^n\| &\le \|\sigma_h^n - \mathcal{P}^h \sigma^n\| + \|\mathcal{P}^h \sigma^n - \sigma^n\| := \|\zeta_\sigma^n\| + \|\ell_\sigma^n\|. \end{aligned} \tag{4.34}$$

According to the approximation properties of the projection operator $\mathcal{P}^h$ given by Lemma 4.1, the projection errors satisfy

$$\|\varrho_u^n\| \le Ch^{k+1}|u^n|_{k+1}, \quad \|\ell_\sigma^n\| \le Ch^{k+1}|\sigma^n|_{k+1}. \tag{4.35}$$

Based on the fully discrete scheme (3.4), similar as with (4.7)–(4.9), we have

$$\begin{aligned} & m_h(\delta_t^\alpha \vartheta_u^{n-\frac{\alpha}{2}}, \vartheta_u^{n-\frac{\alpha}{2}}) + \Delta t^{-\alpha} \sum_{k=0}^{n} w_k^{(\alpha)} a_h(\vartheta_u^{n-k-\frac{\alpha}{2}}, \vartheta_u^{n-\frac{\alpha}{2}}) + a_h(\vartheta_u^{n-\frac{\alpha}{2}}, \vartheta_u^{n-\frac{\alpha}{2}}) + m_h(\zeta_\sigma^{n-\frac{\alpha}{2}}, \zeta_\sigma^{n-\frac{\alpha}{2}}) \\ &= \Big(\Pi_k^{0,h} f(\Pi_k^{0,H} u_H^{n-\frac{\alpha}{2}}) + \Pi_k^{0,h} f'(\Pi_k^{0,H} u_H^{n-\frac{\alpha}{2}})(\Pi_k^{0,h} u_h^{n-\frac{\alpha}{2}} - \Pi_k^{0,H} u_H^{n-\frac{\alpha}{2}}), \vartheta_u^{n-\frac{\alpha}{2}}\Big) - (f(u^{n-\frac{\alpha}{2}}), \vartheta_u^{n-\frac{\alpha}{2}}) \\ &\quad + (g_h^{n-\frac{\alpha}{2}}, \vartheta_u^{n-\frac{\alpha}{2}}) - (g^{n-\frac{\alpha}{2}}, \vartheta_u^{n-\frac{\alpha}{2}}) + (u_t^{n-\frac{\alpha}{2}}, \vartheta_u^{n-\frac{\alpha}{2}}) - m_h(\delta_t^\alpha \mathcal{P}^h u^{n-\frac{\alpha}{2}}, \vartheta_u^{n-\frac{\alpha}{2}}) \\ &\quad + (\sigma^{n-\frac{\alpha}{2}}, \zeta_\sigma^{n-\frac{\alpha}{2}}) - m_h(\mathcal{P}^h \sigma^{n-\frac{\alpha}{2}}, \zeta_\sigma^{n-\frac{\alpha}{2}}) := \mathscr{C}_1^n + \mathscr{C}_2^n + \mathscr{C}_3^n + \mathscr{C}_4^n. \end{aligned} \tag{4.36}$$

To bound $\mathscr{C}_1^n$, we take the Taylor expansion of $f(u^{n-\frac{\alpha}{2}})$ at $\Pi_k^{0,H} u_H^{n-\frac{\alpha}{2}}$:

$$f(u^{n-\frac{\alpha}{2}}) = f(\Pi_k^{0,H} u_H^{n-\frac{\alpha}{2}}) + f'(\Pi_k^{0,H} u_H^{n-\frac{\alpha}{2}})(u^{n-\frac{\alpha}{2}} - \Pi_k^{0,H} u_H^{n-\frac{\alpha}{2}}) + \frac{1}{2} f''(\hat{u})(u^{n-\frac{\alpha}{2}} - \Pi_k^{0,H} u_H^{n-\frac{\alpha}{2}})^2, \tag{4.37}$$

where $\hat{u}$ is between $u^{n-\frac{\alpha}{2}}$ and $\Pi_k^{0,H} u_H^{n-\frac{\alpha}{2}}$. Moreover, according to (2.22), we also get

$$(f(u^{n-\frac{\alpha}{2}}), \Pi_k^{0,h} \vartheta_u^{n-\frac{\alpha}{2}})_K = (\Pi_k^{0,h} f(u^{n-\frac{\alpha}{2}}), \Pi_k^{0,h} \vartheta_u^{n-\frac{\alpha}{2}})_K = (\Pi_k^{0,h} f(u^{n-\frac{\alpha}{2}}), \vartheta_u^{n-\frac{\alpha}{2}})_K. \tag{4.38}$$

By using (4.37) and (4.38), we obtain

$$\begin{aligned} |\mathscr{C}_1^n| &= |\Big(f(\Pi_k^{0,H} u_H^{n-\frac{\alpha}{2}}) + f'(\Pi_k^{0,H} u_H^{n-\frac{\alpha}{2}})(\Pi_k^{0,h} u_h^{n-\frac{\alpha}{2}} - \Pi_k^{0,H} u_H^{n-\frac{\alpha}{2}}), \Pi_k^{0,h} \vartheta_u^{n-\frac{\alpha}{2}}\Big) - (f(u^{n-\frac{\alpha}{2}}), \vartheta_u^{n-\frac{\alpha}{2}})| \\ &= |\Big(f'(\Pi_k^{0,H} u_H^{n-\frac{\alpha}{2}})(\Pi_k^{0,h} u_h^{n-\frac{\alpha}{2}} - u^{n-\frac{\alpha}{2}}) - \frac{1}{2} f''(\hat{u})(u^{n-\frac{\alpha}{2}} - \Pi_k^{0,H} u_H^{n-\frac{\alpha}{2}})^2, \Pi_k^{0,h} \vartheta_u^{n-\frac{\alpha}{2}}\Big) \\ &\quad + (\Pi_k^{0,h} f(u^{n-\frac{\alpha}{2}}) - f(u^{n-\frac{\alpha}{2}}), \vartheta_u^{n-\frac{\alpha}{2}})|. \end{aligned} \tag{4.39}$$

Furthermore, by (2.10), (4.35), and $|f(u)| + |f'(u)| + |f''(u)| \le M$, we get

$$\begin{aligned} |\mathscr{C}_1^n| &\le (\|f'(\Pi_k^{0,H} u_H^{n-\frac{\alpha}{2}})\|_{0,\infty}(\|\Pi_k^{0,h} u_h^{n-\frac{\alpha}{2}} - \Pi_k^{0,h} u^{n-\frac{\alpha}{2}}\| + \|\Pi_k^{0,h} u^{n-\frac{\alpha}{2}} - u^{n-\frac{\alpha}{2}}\|) \\ &\quad + \|\frac{1}{2} f''(\hat{u})\|_{0,\infty}\|(u^{n-\frac{\alpha}{2}} - \Pi_k^{0,H} u_H^{n-\frac{\alpha}{2}})^2\| + \|\Pi_k^{0,h} f(u^{n-\frac{\alpha}{2}}) - f(u^{n-\frac{\alpha}{2}})\|)\|\vartheta_u^{n-\frac{\alpha}{2}}\| \\ &\le M(\|\vartheta_u^{n-\frac{\alpha}{2}}\| + Ch^{k+1}(|u^{n-\frac{\alpha}{2}}|_{k+1} + |f(u^{n-\frac{\alpha}{2}})|_{k+1}) + \|u^{n-\frac{\alpha}{2}} - \Pi_k^{0,H} u^{n-\frac{\alpha}{2}}\|_{0,4}^2 \\ &\quad + \|\Pi_k^{0,H} u^{n-\frac{\alpha}{2}} - \Pi_k^{0,H} u_H^{n-\frac{\alpha}{2}}\|_{0,4}^2)\|\vartheta_u^{n-\frac{\alpha}{2}}\|. \end{aligned} \tag{4.40}$$

Thus, for the term $\mathscr{C}_1^n$, by using Lemmas 4.2 and 4.4, we obtain

$$\begin{aligned} |\mathscr{C}_1^n| &\le M(\|\vartheta_u^{n-\frac{\alpha}{2}}\| + Ch^{k+1}(|u^{n-\frac{\alpha}{2}}|_{k+1} + |f(u^{n-\frac{\alpha}{2}})|_{k+1}) + CH^{2k+2}|u^{n-\frac{\alpha}{2}}|_{k+1,4}^2 \\ &\quad + C\|u^{n-\frac{\alpha}{2}} - u_H^{n-\frac{\alpha}{2}}\|\|\|\nabla u^{n-\frac{\alpha}{2}} - \nabla u_H^{n-\frac{\alpha}{2}}\|)\|\vartheta_u^{n-\frac{\alpha}{2}}\|. \end{aligned} \tag{4.41}$$

Using the Cauchy-Schwarz inequality and (2.11), we derive

$$|\mathscr{C}_2^n| = |(g_h^{n-\frac{\alpha}{2}} - g^{n-\frac{\alpha}{2}}, \vartheta_u^{n-\frac{\alpha}{2}})| = |(\Pi_k^{0,h} g^{n-\frac{\alpha}{2}} - g^{n-\frac{\alpha}{2}}, \vartheta_u^{n-\frac{\alpha}{2}})| \leq Ch^{k+1}|g^{n-\frac{\alpha}{2}}|_{k+1}\|\vartheta_u^{n-\frac{\alpha}{2}}\|. \tag{4.42}$$

Simlar as with (4.13), for the term $\mathscr{C}_3^n$, we have the following estimate:

$$\begin{aligned}|\mathscr{C}_3^n| &= |(u_t^{n-\frac{\alpha}{2}}, \vartheta_u^{n-\frac{\alpha}{2}}) - m_h(\delta_t^\alpha \mathcal{P}^h u^{n-\frac{\alpha}{2}}, \vartheta_u^{n-\frac{\alpha}{2}})| \\ &\leq C(\Delta t^2\|u_{ttt}\|_{L^1(0,t_n,L^2(\Omega))} + h^{k+1}\|u_t\|_{L^1(0,t_n,H^{k+1}(\Omega))})\|\vartheta_u^{n-\frac{\alpha}{2}}\|.\end{aligned} \tag{4.43}$$

Meanwhile, by virtue of (4.14), for the term $\mathscr{C}_4^n$, it holds that:

$$|\mathscr{C}_4^n| = |(\sigma^{n-\frac{\alpha}{2}}, \zeta_\sigma^{n-\frac{\alpha}{2}}) - m_h(\mathcal{P}^h\sigma^{n-\frac{\alpha}{2}}, \zeta_\sigma^{n-\frac{\alpha}{2}})| \leq C_{\mathfrak{J}^*}h^{k+1}|\sigma^{n-\frac{\alpha}{2}}|_{k+1}\|\zeta_\sigma^{n-\frac{\alpha}{2}}\|. \tag{4.44}$$

Using (2.15), (4.16), and Lemma 3.1, substituting (4.41)–(4.44) into (4.36), and summing for n from 2 to m, we get

$$\begin{aligned}&\frac{\mathscr{F}(\vartheta_u^m) - \mathscr{F}(\vartheta_u^1)}{4\Delta t} + \Delta t^{-\alpha}\sum_{n=2}^m\sum_{k=0}^n w_k^{(\alpha)} a_h(\vartheta_u^{n-k-\frac{\alpha}{2}}, \vartheta_u^{n-\frac{\alpha}{2}}) + \sum_{n=2}^m(\|\nabla\vartheta_u^{n-\frac{\alpha}{2}}\|_h^2 + \|\zeta_\sigma^{n-\frac{\alpha}{2}}\|_h^2) \\ &\leq \sum_{n=2}^m C^*(\|\vartheta_u^{n-\frac{\alpha}{2}}\| + \Delta t^2\|u_{ttt}\|_{L^1(0,t_n,L^2(\Omega))} + h^{k+1}K_0 + H^{2k+2}|u^{n-\frac{\alpha}{2}}|_{k+1,4}^2 \\ &\quad + \|u^{n-\frac{\alpha}{2}} - u_H^{n-\frac{\alpha}{2}}\|\|\nabla u^{n-\frac{\alpha}{2}} - \nabla u_H^{n-\frac{\alpha}{2}}\|)\|\vartheta_u^{n-\frac{\alpha}{2}}\| + \sum_{n=2}^m C_{\mathfrak{J}^*}h^{k+1}|\sigma^{n-\frac{\alpha}{2}}|_{k+1}\|\zeta_\sigma^{n-\frac{\alpha}{2}}\|,\end{aligned} \tag{4.45}$$

where C^* is independent of h, H, and Δt, and depends on M. Multiplying (4.45) by $4\Delta t$ and applying (3.1), we obtain

$$\begin{aligned}&\|\vartheta_u^m\|_h^2 + 4\Delta t^{1-\alpha}\sum_{n=2}^m\sum_{k=0}^n w_k^{(\alpha)} a_h(\vartheta_u^{n-k-\frac{\alpha}{2}}, \vartheta_u^{n-\frac{\alpha}{2}}) + 4\Delta t\sum_{n=2}^m(\|\nabla\vartheta_u^{n-\frac{\alpha}{2}}\|_h^2 + \|\zeta_\sigma^{n-\frac{\alpha}{2}}\|_h^2) \\ &\leq 7\|\vartheta_u^1\|_h^2 + 4\|\vartheta_u^0\|_h^2 + C\Delta t\sum_{n=2}^m(\|\vartheta_u^{n-\frac{\alpha}{2}}\| + \Delta t^2\|u_{ttt}\|_{L^1(0,t_n,L^2(\Omega))} + h^{k+1}K_0 + H^{2k+2}|u^{n-\frac{\alpha}{2}}|_{k+1,4}^2 \\ &\quad + \|u^{n-\frac{\alpha}{2}} - u_H^{n-\frac{\alpha}{2}}\|\|\nabla u^{n-\frac{\alpha}{2}} - \nabla u_H^{n-\frac{\alpha}{2}}\|)\|\vartheta_u^{n-\frac{\alpha}{2}}\| + 4\Delta t\sum_{n=2}^m C_{\mathfrak{J}^*}h^{k+1}|\sigma^{n-\frac{\alpha}{2}}|_{k+1}\|\zeta_\sigma^{n-\frac{\alpha}{2}}\|.\end{aligned} \tag{4.46}$$

For $n = 1$, we make use of a similar process as with the case where $n \geq 2$ to arrive at

$$\begin{aligned}&\frac{1}{2}\delta_t\|\vartheta_u^1\|_h^2 + \frac{(1-\alpha)\Delta t}{2}\|\delta_t\vartheta_u^1\|_h^2 + \Delta t^{-\alpha}\sum_{k=0}^1 w_k^{(\alpha)} a_h(\vartheta_u^{1-k-\frac{\alpha}{2}}, \vartheta_u^{1-\frac{\alpha}{2}}) + \|\nabla\vartheta_u^{1-\frac{\alpha}{2}}\|_h^2 + \|\zeta_\sigma^{1-\frac{\alpha}{2}}\|_h^2 \\ &\leq C^*(\|\vartheta_u^{1-\frac{\alpha}{2}}\| + \Delta t^2\|u_{ttt}\|_{L^1(0,t_1,L^2(\Omega))} + h^{k+1}K_0 + H^{2k+2}|u^{1-\frac{\alpha}{2}}|_{k+1,4}^2 \\ &\quad + \|u^{1-\frac{\alpha}{2}} - u_H^{1-\frac{\alpha}{2}}\|\|\nabla u^{1-\frac{\alpha}{2}} - \nabla u_H^{1-\frac{\alpha}{2}}\|)\|\vartheta_u^{1-\frac{\alpha}{2}}\| + C_{\mathfrak{J}^*}h^{k+1}|\sigma^{1-\frac{\alpha}{2}}|_{k+1}\|\zeta_\sigma^{1-\frac{\alpha}{2}}\|.\end{aligned} \tag{4.47}$$

Then, removing the positive term $\frac{(1-\alpha)\Delta t}{2}\|\delta_t\vartheta_u^1\|_h^2$, multiplying (4.47) by $2\Delta t$, and combining (4.46) with the estimate $\|u^{n-\frac{\alpha}{2}} - u_H^{n-\frac{\alpha}{2}}\| \leq C(\Delta t^2 + H^{k+1})$ of Theorem 4.1, as well as, by using the Young inequality, it holds that

$$\begin{aligned}&\|\vartheta_u^m\|_h^2+4\Delta t^{1-\alpha}\sum_{n=1}^{m}\sum_{k=0}^{n}w_k^{(\alpha)}a_h(\vartheta_u^{n-k-\frac{\alpha}{2}},\vartheta_u^{n-\frac{\alpha}{2}})+4\Delta t\sum_{n=1}^{m}(\|\nabla\vartheta_u^{n-\frac{\alpha}{2}}\|_h^2+\|\zeta_\sigma^{n-\frac{\alpha}{2}}\|_h^2)\\ &\le C\|\vartheta_u^0\|_h^2+C_*\Delta t\sum_{n=1}^{m}\|\vartheta_u^{n-\frac{\alpha}{2}}\|^2+C_T(\Delta t^2\|u_{ttt}\|_{L^1(0,t_n,L^2(\Omega))}+h^{k+1}(K_0+C_{\mathfrak{J}^*}|\sigma^{n-\frac{\alpha}{2}}|_{k+1})\\ &\quad+H^{2k+2}|u^{n-\frac{\alpha}{2}}|_{k+1,4}^2)^2+(\Delta t^2+H^{k+1})^2\Big(\Delta t\sum_{n=1}^{m}\|\nabla u^{n-\frac{\alpha}{2}}-\nabla u_H^{n-\frac{\alpha}{2}}\|^2\Big)+2\Delta t\sum_{n=1}^{m}\|\zeta_\sigma^{n-\frac{\alpha}{2}}\|^2.\end{aligned}\tag{4.48}$$

According to the equivalent norms $\|\cdot\|$, and $\|\cdot\|_h$, and $\|\vartheta_u^0\|=0$, and using Theorem 4.1, the discrete Grönwall inequality, Lemma 3.2, (4.34), and (4.35), we finish the proof. □

5. Numerical example

In this section, we will present an experiment to verify the correctness of our theoretical optimal convergence rates using the two-grid MVEM. The practical calculations of the example are carried out on the Voronoi-Lloyd meshes, the distort Voronoi-Lloyd meshes, the non-convex meshes, and the distorted square meshes shown in Figure 1 (see [36]). Moreover, we also provide the refined meshes in Figure 2. Due to the basis functions being defined by $\mathrm{dof}_i(\varphi_j)=\delta_{ij}, i,j=1,\ldots,N^{\mathrm{dof}}$, which are unknown functions inside the elements, we compute the L^2-norm errors by using the local projection operator $\Pi_{k,K}^0$:

$$\mathrm{error}\,(\mathbf{u}):=\left(\sum_{K\in\mathcal{T}_h}\left\|\mathbf{u}(T)-\Pi_{k,K}^0\mathbf{u_h}^m\right\|_K^2\right)^{\frac{1}{2}},\mathrm{error}\,(\sigma):=\left(\sum_{K\in\mathcal{T}_h}\left\|\sigma(T)-\Pi_{k,K}^0\sigma_{\mathbf{h}}{}^m\right\|_K^2\right)^{\frac{1}{2}}.\tag{5.1}$$

In order to demonstrate the effectiveness and accuracy of the two-grid MVEM, we consider the following problem:

$$\begin{cases}\frac{\partial u}{\partial t}-\frac{\partial^\alpha\Delta u}{\partial t^\alpha}-\Delta u+\Delta^2u=f(u)+g(\mathbf{x},t), & (\mathbf{x},t)\in\Omega\times J,\\ u(\mathbf{x},t)=\Delta u(\mathbf{x},t)=0, & (\mathbf{x},t)\in\partial\Omega\times J,\\ u(\mathbf{x},0)=u_0(\mathbf{x}), & \mathbf{x}\in\Omega.\end{cases}\tag{5.2}$$

With the nonlinear term $f(u)=u^2$, the space-time domain $[0,1]^2\times[0,1]$, the known source term $g(\mathbf{x},t)$

$$g(\mathbf{x},t)=\left(2t+8\pi^2t^2+64\pi^4t^2+\frac{16\pi^2t^2}{\Gamma(3-\alpha)}\right)\sin(2\pi x)\sin(2\pi y)-t^4\sin^2(2\pi x)\sin^2(2\pi y),\tag{5.3}$$

we have the following exact solution for this example:

$$u=t^2\sin(2\pi x)\sin(2\pi y).\tag{5.4}$$

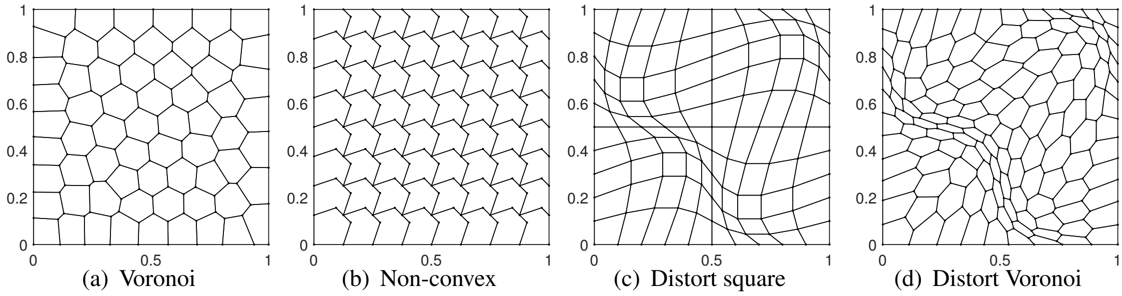

Figure 1. Different polygon coarse meshes.

Table 1. L^2-norm errors and space convergence rates on the Voronoi-Lloyd meshes with $k = 1$.

α	H	h	$\|\|u - u_h\|\|$	Order$_u$	$\|\|\sigma - \sigma_h\|\|$	Order$_\sigma$	CPU time (s)
0.05	1.7678E-01	7.6472E-02	4.5579E-02	-	1.2630E+00	-	0.44
	1.2910E-01	5.4965E-02	2.5248E-02	1.7888	6.2997E-01	2.1064	0.67
	8.8388E-02	3.7113E-02	1.1283E-02	2.0510	2.6617E-01	2.1938	1.46
	6.2500E-02	2.6011E-02	5.5204E-03	2.0111	1.2499E-01	2.1266	4.35
	4.4194E-02	1.8291E-02	2.7452E-03	1.9839	6.0098E-02	2.0796	12.84
0.25	1.7678E-01	7.6472E-02	4.5505E-02	-	1.2570E+00	-	0.35
	1.2910E-01	5.4965E-02	2.5199E-02	1.7897	6.2616E-01	2.1103	0.60
	8.8388E-02	3.7113E-02	1.1255E-02	2.0525	2.6401E-01	2.1991	1.41
	6.2500E-02	2.6011E-02	5.5010E-03	2.0139	1.2353E-01	2.1368	4.34
	4.4194E-02	1.8291E-02	2.7304E-03	1.9894	5.8965E-02	2.1002	12.60
0.50	1.7678E-01	7.6472E-02	4.5416E-02	-	1.2497E+00	-	0.35
	1.2910E-01	5.4965E-02	2.5145E-02	1.7903	6.2196E-01	2.1131	0.58
	8.8388E-02	3.7113E-02	1.1229E-02	2.0529	2.6203E-01	2.2011	1.44
	6.2500E-02	2.6011E-02	5.4873E-03	2.0145	1.2250E-01	2.1392	4.32
	4.4194E-02	1.8291E-02	2.7229E-03	1.9900	5.8400E-02	2.1038	12.52
0.75	1.7678E-01	7.6472E-02	4.5348E-02	-	1.2442E+00	-	0.35
	1.2910E-01	5.4965E-02	2.5116E-02	1.7892	6.1971E-01	2.1107	0.58
	8.8388E-02	3.7113E-02	1.1230E-02	2.0495	2.6216E-01	2.1906	1.42
	6.2500E-02	2.6011E-02	5.5020E-03	2.0074	1.2362E-01	2.1149	4.31
	4.4194E-02	1.8291E-02	2.7446E-03	1.9751	6.0052E-02	2.0504	12.52
0.95	1.7678E-01	7.6472E-02	4.5324E-02	-	1.2423E+00	-	0.35
	1.2910E-01	5.4965E-02	2.5125E-02	1.7866	6.2041E-01	2.1026	0.58
	8.8388E-02	3.7113E-02	1.1265E-02	2.0426	2.6479E-01	2.1681	1.44
	6.2500E-02	2.6011E-02	5.5469E-03	1.9931	1.2704E-01	2.0662	4.21
	4.4194E-02	1.8291E-02	2.7954E-03	1.9461	6.3947E-02	1.9495	12.27

Table 2. L^2-norm errors and space convergence rates on the disortion square meshes with $k = 1$.

α	H	h	$\|\|u - u_h\|\|$	Order_u	$\|\|\sigma - \sigma_h\|\|$	Order_σ	CPU time (s)
0.05	2.0000E-01	1.0000E-01	1.2546E-01	-	3.1109E+00	-	0.28
	1.0000E-01	5.0000E-02	4.2232E-02	1.5708	1.0175E+00	1.6123	0.67
	6.6667E-02	3.3333E-02	1.9979E-02	1.8461	4.7210E-01	1.8939	1.60
	5.0000E-02	2.5000E-02	1.1493E-02	1.9221	2.6940E-01	1.9501	3.90
	4.0000E-02	2.0000E-02	7.4321E-03	1.9535	1.7347E-01	1.9725	7.51
0.25	2.0000E-01	1.0000E-01	1.2489E-01	-	3.0998E+00	-	0.20
	1.0000E-01	5.0000E-02	4.2034E-02	1.5710	1.0138E+00	1.6124	0.66
	6.6667E-02	3.3333E-02	1.9882E-02	1.8464	4.7020E-01	1.8948	1.58
	5.0000E-02	2.5000E-02	1.1435E-02	1.9229	2.6821E-01	1.9515	3.87
	4.0000E-02	2.0000E-02	7.3924E-03	1.9548	1.7263E-01	1.9745	7.43
0.50	2.0000E-01	1.0000E-01	1.2412E-01	-	3.0850E+00	-	0.21
	1.0000E-01	5.0000E-02	4.1774E-02	1.5710	1.0090E+00	1.6123	0.68
	6.6667E-02	3.3333E-02	1.9759E-02	1.8464	4.6791E-01	1.8952	1.60
	5.0000E-02	2.5000E-02	1.1364E-02	1.9230	2.6688E-01	1.9518	3.90
	4.0000E-02	2.0000E-02	7.3462E-03	1.9549	1.7176E-01	1.9749	7.40
0.75	2.0000E-01	1.0000E-01	1.2331E-01	-	3.0703E+00	-	0.20
	1.0000E-01	5.0000E-02	4.1515E-02	1.5706	1.0047E+00	1.6116	0.65
	6.6667E-02	3.3333E-02	1.9646E-02	1.8452	4.6613E-01	1.8940	1.56
	5.0000E-02	2.5000E-02	1.1306E-02	1.9207	2.6608E-01	1.9489	3.87
	4.0000E-02	2.0000E-02	7.3148E-03	1.9513	1.7145E-01	1.9698	7.52
0.95	2.0000E-01	1.0000E-01	1.2267E-01	-	3.0592E+00	-	0.20
	1.0000E-01	5.0000E-02	4.1323E-02	1.5698	1.0019E+00	1.6104	0.63
	6.6667E-02	3.3333E-02	1.9573E-02	1.8429	4.6540E-01	1.8911	1.57
	5.0000E-02	2.5000E-02	1.1278E-02	1.9163	2.6616E-01	1.9424	3.80
	4.0000E-02	2.0000E-02	7.3091E-03	1.9439	1.7193E-01	1.9585	7.34

Next, we show the L^2-norm errors and space convergence orders for u and σ using the two-grid MVEM with polynomial degrees $k = 1$ and $k = 2$ on four kinds of meshes and their refined meshes(i.e., Voronoi meshes, distorted square meshes, distorted Voronoi meshes, and non-convex meshes, respectively) based on a fixed time step of $\Delta t = 10^{-2}$, varying two-grid sizes H, h, and changed fractional order parameters α from $0.05, 0.25, 0.5, 0.75$ to 0.95 in Tables 1–6. In Tables 7–8, we compare the performance of the two-grid MVEM with $k = 1$ and $k = 2$ against the Newton iteration method in solving equations (5.2) on four different meshes, using a fixed time step $\Delta t = 10^{-2}$, fractional parameter $\alpha = 0.05$, and $T = 1$. In order to observe the numerical simulation results of the two-grid MVEM more intuitively, we also provide the function graphs of the numerical solutions u_h and σ_h in Figures 3–8 at $t = 1$. The CPU time presented in the tables is reported in seconds.

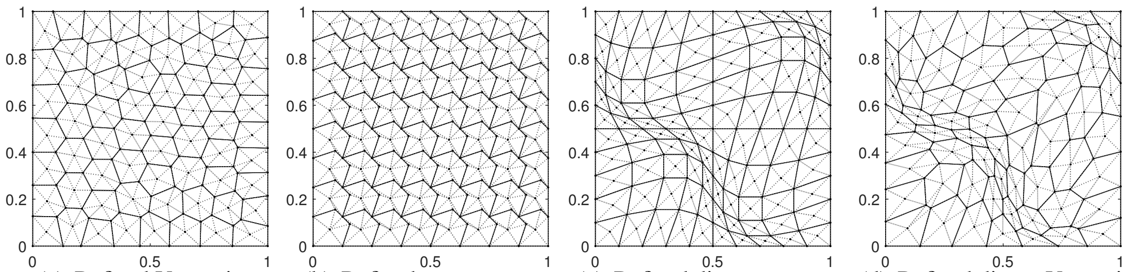

(a) Refined Voronoi (b) Refined non-convex (c) Refined distort square (d) Refined distort Voronoi

Figure 2. Corresponding refined polygon meshes.

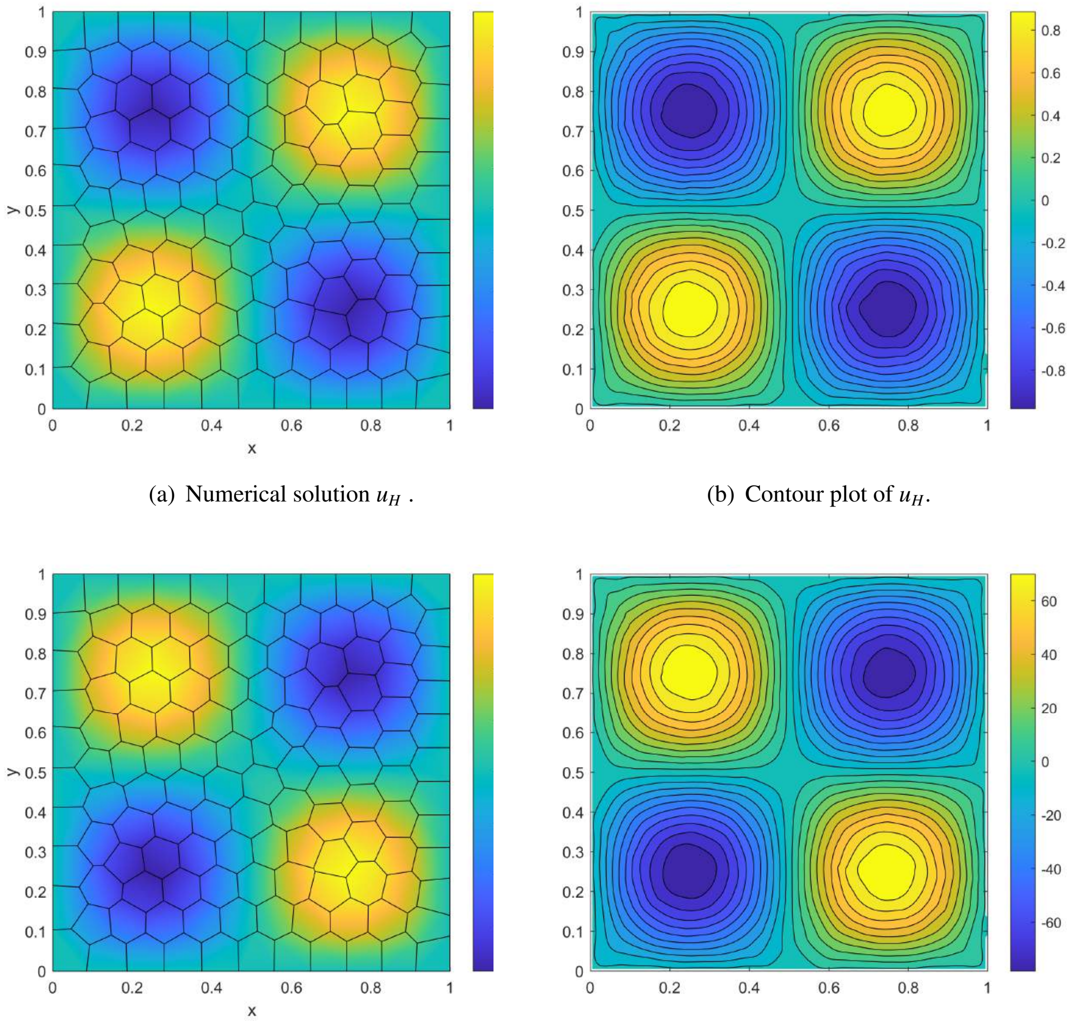

(a) Numerical solution u_H . (b) Contour plot of u_H.

(c) Numerical solution σ_H. (d) Contour plot of σ_H.

Figure 3. Numerical solutions u_H and σ_H on the coarse Voronoi meshes with $\alpha = 0.05$ at $t = 1$.

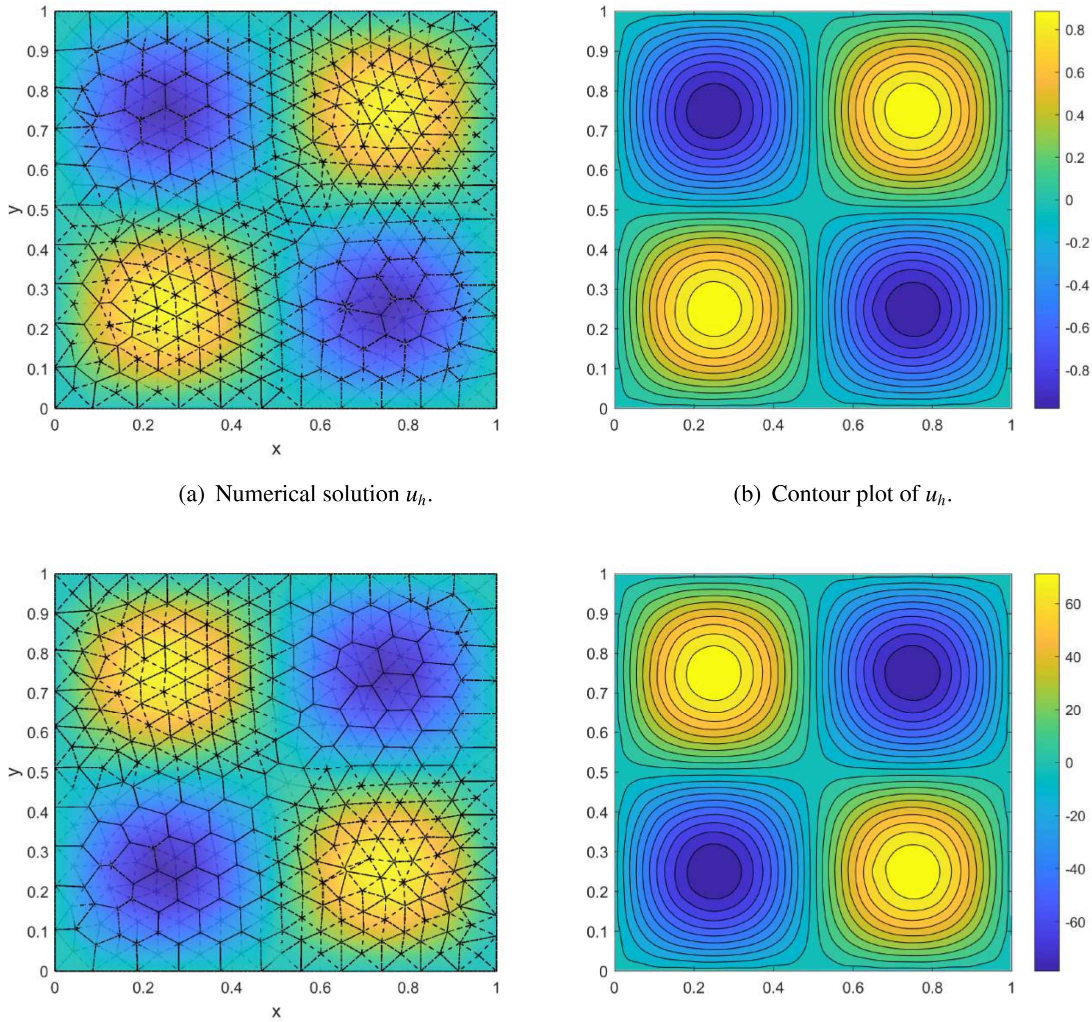

(a) Numerical solution u_h.

(b) Contour plot of u_h.

(c) Numerical solution σ_h.

(d) Contour plot of σ_h.

Figure 4. Numerical solutions u_h and σ_h on the refined Voronoi meshes with $\alpha = 0.05$ at $t = 1$.

The results of Tables 1–4 show that the spatial convergence order is close to 2 on complex polygon meshes with $k = 1$. It is easy to see that the two-grid MVEM can achieve optimal convergence results and has good numerical simulation performance. As shown in Table 7, under the given parameters and meshes, both methods yield nearly identical errors for u and σ, proving the two-grid MVEM successfully captures the solution accuracy achievable with the Newton iterative method. Meanwhile, we can find that the two-grid MVEM significantly reduces the computational cost while maintaining the same accuracy across all meshes, such as achieving a 15.2% reduction (10.83 s vs. 12.77 s) for the Voronoi-Lloyd mesh, 12.5% reduction (39.17 s vs. 44.74 s) for the distorted Voronoi mesh, 35.7% reduction (5.71 s vs. 8.88 s) for the distorted square mesh, and 7.8% reduction (5.84 s vs. 6.33 s) for the non-convex mesh.

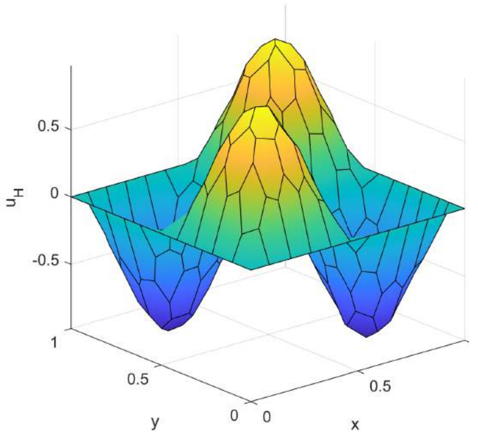

(a) Numerical solution u_H.

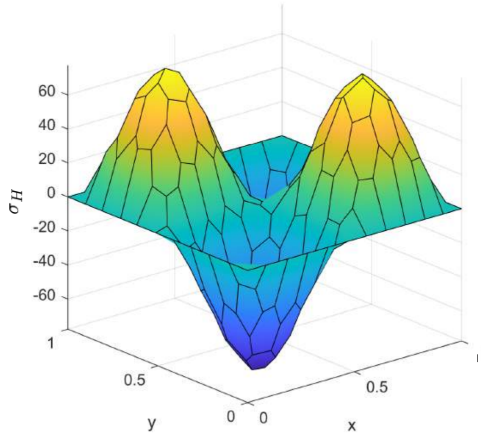

(b) Numerical solution σ_H.

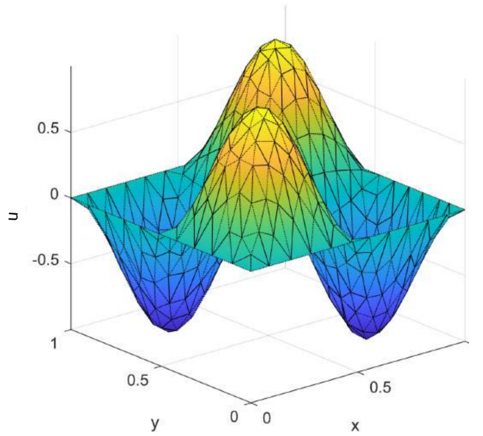

(c) Exact solution u.

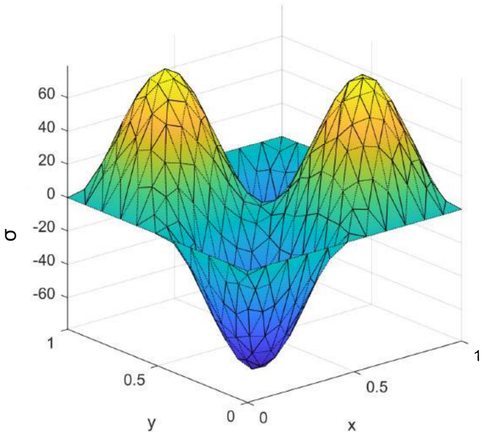

(d) Exact solution σ.

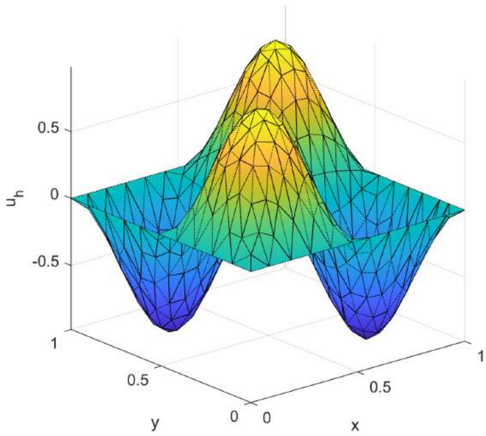

(e) Numerical solution u_h.

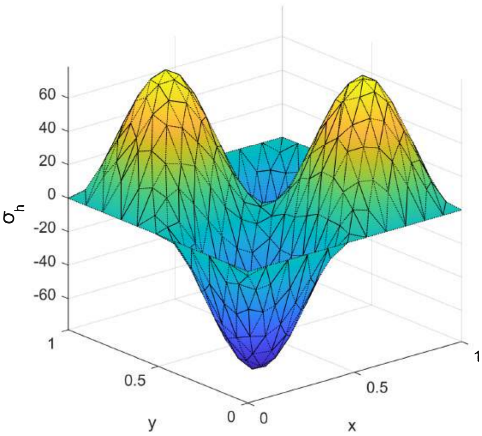

(f) Numerical solution σ_h.

Figure 5. Exact solution and numerical solution on the coarse and refined Voronoi meshes with $\alpha = 0.05$ at $t = 1$.

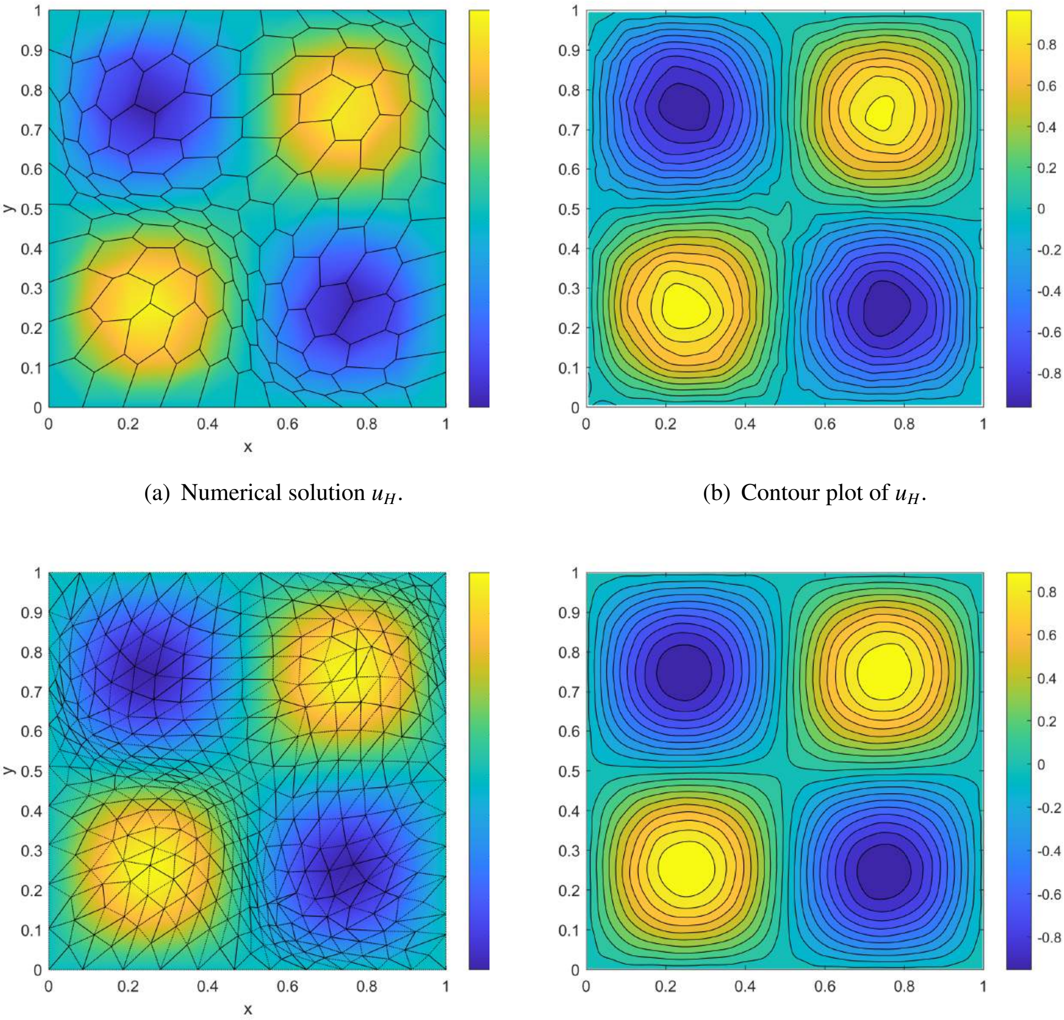

(a) Numerical solution u_H.

(b) Contour plot of u_H.

(c) Numerical solution u_h.

(d) Contour plot of u_h.

Figure 6. u_H and u_h on the coarse and refined distorted Voronoi meshes with $\alpha = 0.25$ at $t = 1$.

In Tables 5–6, we present the L^2-norm errors and convergence rates of the two-grid MVEM with $k = 2$ on the Voronoi-Lloyd and non-convex meshes for several fractional parameters $\alpha = 0.05, 0.25, 0.5, 0.75,$ and 0.95. As the meshes are refined, the errors $\|u - u_h\|$ and $\|\sigma - \sigma_h\|$ decrease for all tested α. In Table 8, we compare the proposed two-grid MVEM with the Newton iterative method performed directly on the refined meshes. The key observation is that the two-grid MVEM achieves the same accuracy as the fine-grid Newton method, but with noticeably reduced CPU times, such as achieving a 58.6% reduction (58.15 s vs. 92.18 s) for the Voronoi-Lloyd mesh, 54.6% reduction (208.80 s vs. 322.90 s) for the distorted Voronoi mesh, 100.1% reduction (52.54 s vs. 107.60 s) for the distorted square mesh, and 44.1% reduction (25.54 s vs. 36.78 s) for the non-convex mesh.

When the projection polynomial degree is $k = 2$, the degrees of freedom include not only boundary degrees of freedom but also additional internal degrees of freedom. This increases the size of the coupled system on the fine grid and raises both the assembly cost and the cost of a single linear computation. Consequently, although the high-order approximation in space can substantially improve numerical accuracy, it also incurs a higher computational expense. For example, we can see from Tables 7–8 on the Voronoi–Lloyd mesh that the two-grid MVEM CPU time increases from 10.83 s ($k = 1$) to 58.15 s ($k = 2$), while $\|u - u_h\|$ decreases from 2.7452×10^{-3} to 5.0281×10^{-5} and $\|\sigma - \sigma_h\|$ decreases from 6.0098×10^{-2} to 1.0992×10^{-3}. Moreover, the fine-grid Newton iteration becomes even more expensive when $k = 2$. On the same Voronoi-Lloyd mesh, its CPU time grows from 12.77 s to 92.18 s, which is larger than the growth for the two-grid MVEM. This reflects that the Newton iteration repeatedly assembles and solves the fine-grid linearized system, making it have a higher computing cost based on the high-order space approximation.

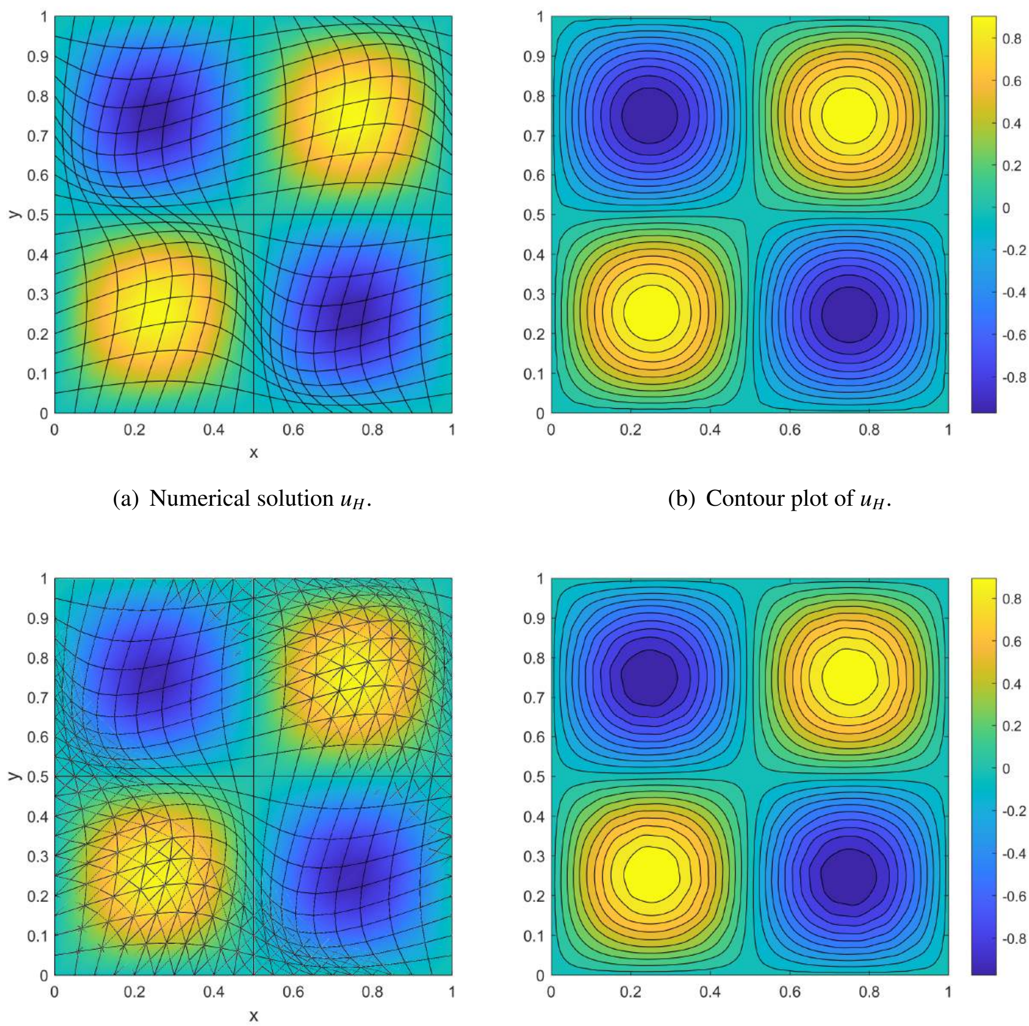

(a) Numerical solution u_H. (b) Contour plot of u_H.

(c) Numerical solution u_h. (d) Contour plot of u_h.

Figure 7. u_H and u_h on the coarse and refined distorted square meshes with $\alpha = 0.5$ at $t = 1$.

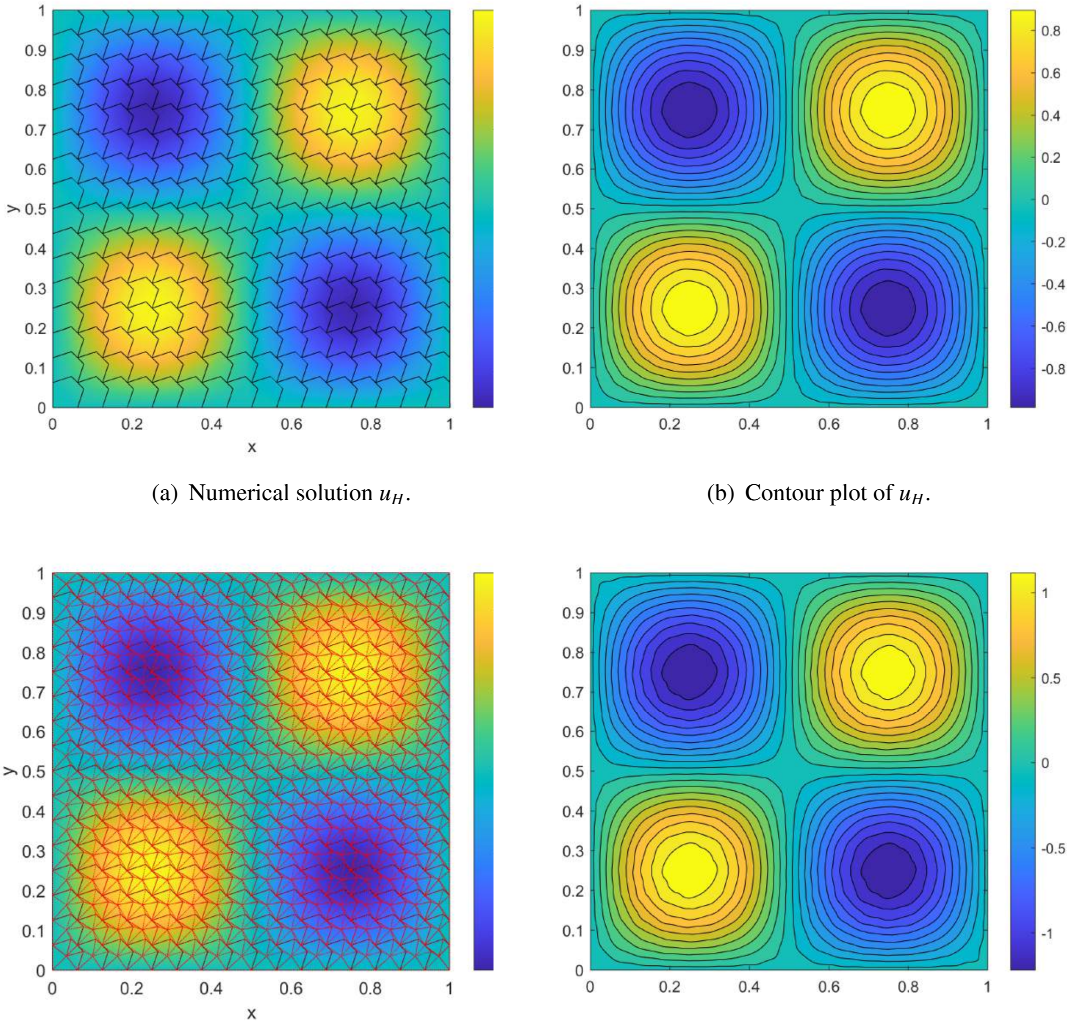

(a) Numerical solution u_H.

(b) Contour plot of u_H.

(c) Numerical solution u_h.

(d) Contour plot of u_h.

Figure 8. u_H and u_h on the coarse and refined non-convex meshes with $\alpha = 0.75$ at $t = 1$.

Table 3. L^2-norm errors and space convergence rates on the non-convex meshes with $k = 1$.

α	H	h	$\|\|u - u_h\|\|$	Order$_u$	$\|\|\sigma - \sigma_h\|\|$	Order$_\sigma$	CPU time (s)
0.05	2.5000E-01	9.4491E-02	1.0139E-01	-	3.0685E+00	-	0.40
	1.2500E-01	4.5644E-02	3.2437E-02	1.5662	8.3928E-01	1.7816	0.91
	6.2500E-02	2.2451E-02	8.7996E-03	1.8387	2.2263E-01	1.8703	6.90
	3.1250E-02	1.1136E-02	2.2542E-03	1.9424	5.6823E-02	1.9476	78.44
0.25	2.5000E-01	9.4491E-02	1.0124E-01	-	3.0573E+00	-	0.28
	1.2500E-01	4.5644E-02	3.2367E-02	1.5672	8.3470E-01	1.7841	0.89
	6.2500E-02	2.2451E-02	8.7732E-03	1.8398	2.2079E-01	1.8742	6.70
	3.1250E-02	1.1136E-02	2.2406E-03	1.9467	5.5767E-02	1.9626	78.75
0.50	2.5000E-01	9.4491E-02	1.0105E-01	-	3.0430E+00	-	0.26
	1.2500E-01	4.5644E-02	3.2284E-02	1.5681	8.2946E-01	1.7863	0.90
	6.2500E-02	2.2451E-02	8.7494E-03	1.8400	2.1929E-01	1.8750	6.77
	3.1250E-02	1.1136E-02	2.2345E-03	1.9468	5.5319E-02	1.9643	78.60
0.75	2.5000E-01	9.4491E-02	1.0086E-01	-	3.0300E+00	-	0.27
	1.2500E-01	4.5644E-02	3.2222E-02	1.5682	8.2617E-01	1.7859	0.87
	6.2500E-02	2.2451E-02	8.7525E-03	1.8369	2.1996E-01	1.8651	6.73
	3.1250E-02	1.1136E-02	2.2565E-03	1.9333	5.7126E-02	1.9228	77.83
0.95	2.5000E-01	9.4491E-02	1.0074E-01	-	3.0218E+00	-	0.27
	1.2500E-01	4.5644E-02	3.2204E-02	1.5673	8.2606E-01	1.7824	0.87
	6.2500E-02	2.2451E-02	8.7869E-03	1.8305	2.2308E-01	1.8451	6.73
	3.1250E-02	1.1136E-02	2.3066E-03	1.9076	6.1179E-02	1.8452	78.02

Table 4. L^2-norm errors and space convergence rates on the distortion Voronoi-Lloyd meshes with $k = 1$.

α	H	h	$\|\|u - u_h\|\|$	Order$_u$	$\|\|\sigma - \sigma_h\|\|$	Order$_\sigma$	CPU time (s)
0.05	1.7678E-01	7.6472E-02	1.0137E-01	-	2.6748E+00	-	0.37
	1.2910E-01	5.4965E-02	4.4431E-02	2.4977	1.1603E+00	2.5293	0.59
	6.2500E-02	2.6011E-02	1.1637E-02	1.7907	2.6599E-01	1.9687	4.36
	4.4194E-02	1.8291E-02	5.5925E-03	2.0809	1.2723E-01	2.0943	12.42
0.25	1.7678E-01	7.6472E-02	1.0098E-01	-	2.6655E+00	-	0.35
	1.2910E-01	5.4965E-02	4.4287E-02	2.4958	1.1557E+00	2.5306	0.58
	6.2500E-02	2.6011E-02	1.1584E-02	1.7925	2.6438E-01	1.9716	4.28
	4.4194E-02	1.8291E-02	5.5643E-03	2.0823	1.2620E-01	2.1002	12.38
0.50	1.7678E-01	7.6472E-02	1.0046E-01	-	2.6533E+00	-	0.34
	1.2910E-01	5.4965E-02	4.4101E-02	2.4929	1.1501E+00	2.5315	0.59
	6.2500E-02	2.6011E-02	1.1521E-02	1.7941	2.6274E-01	1.9734	4.29
	4.4194E-02	1.8291E-02	5.5355E-03	2.0817	1.2539E-01	2.1008	12.31
0.75	1.7678E-01	7.6472E-02	9.9921E-02	-	2.6417E+00	-	0.34

Continued on next page.

α	H	h	$\|u-u_h\|$	Order$_u$	$\|\sigma-\sigma_h\|$	Order$_\sigma$	CPU time (s)
	1.2910E-01	5.4965E-02	4.3927E-02	2.4887	1.1455E+00	2.5302	0.58
	6.2500E-02	2.6011E-02	1.1476E-02	1.7941	2.6222E-01	1.9708	4.19
	4.4194E-02	1.8291E-02	5.5269E-03	2.0748	1.2585E-01	2.0846	12.33
0.95	1.7678E-01	7.6472E-02	9.9504E-02	-	2.6335E+00	-	0.35
	1.2910E-01	5.4965E-02	4.3810E-02	2.4842	1.1434E+00	2.5266	0.58
	6.2500E-02	2.6011E-02	1.1462E-02	1.7922	2.6318E-01	1.9633	4.20
	4.4194E-02	1.8291E-02	5.5447E-03	2.0622	1.2779E-01	2.0517	12.05

Table 5. L^2-norm errors and space convergence rates on the Voronoi-Lloyd meshes with $k = 2$.

α	H	h	$\|u-u_h\|$	Order$_u$	$\|\sigma-\sigma_h\|$	Order$_\sigma$	CPU time (s)
0.05	1.7678E-01	7.6472E-02	3.5852E-03	-	9.5684E-02	-	2.64
	1.2910E-01	5.4965E-02	1.2604E-03	3.1656	3.6359E-02	3.0611	5.03
	8.8388E-02	3.7113E-02	3.9019E-04	2.9857	1.1433E-02	2.8741	13.14
	6.2500E-02	2.6011E-02	1.2042E-04	3.3076	3.7760E-03	2.9521	47.85
0.25	1.7678E-01	7.6472E-02	3.4270E-03	-	9.7309E-02	-	2.10
	1.2910E-01	5.4965E-02	1.3293E-03	2.9660	3.6096E-02	3.0760	4.50
	8.8388E-02	3.7113E-02	4.2148E-04	3.0654	1.1865E-02	2.8246	12.69
	6.2500E-02	2.6011E-02	1.2761E-04	3.3675	3.9128E-03	2.9160	47.74
0.50	1.7678E-01	7.6472E-02	3.3424E-03	-	9.6381E-02	-	2.10
	1.2910E-01	5.4965E-02	1.2701E-03	3.0827	3.5788E-02	3.0610	4.35
	8.8388E-02	3.7113E-02	4.0962E-04	3.0035	1.1690E-02	2.8205	12.96
	6.2500E-02	2.6011E-02	1.2492E-04	3.2553	3.8796E-03	2.8989	47.52
0.75	1.7678E-01	7.6472E-02	3.6240E-03	-	9.8927E-02	-	2.01
	1.2910E-01	5.4965E-02	1.3258E-03	3.2252	3.6807E-02	3.0767	4.35
	8.8388E-02	3.7113E-02	4.0933E-04	3.1305	1.1974E-02	2.8597	12.78
	6.2500E-02	2.6011E-02	1.2540E-04	3.2307	3.9663E-03	2.9198	47.41
0.95	1.7678E-01	7.6472E-02	3.5714E-03	-	9.2804E-02	-	2.10
	1.2910E-01	5.4965E-02	1.3009E-03	3.1925	3.4946E-02	3.0098	4.35
	8.8388E-02	3.7113E-02	4.0828E-04	3.0844	1.1467E-02	2.8434	12.96
	6.2500E-02	2.6011E-02	1.2587E-04	3.2106	3.8211E-03	2.8711	46.31

Table 6. L^2-norm errors and space convergence rates on the non-convex meshes with $k = 2$.

α	H	h	$\|\|u - u_h\|\|$	Order_u	$\|\|\sigma - \sigma_h\|\|$	Order_σ	CPU time (s)
0.05	2.5000E-01	9.4491E-02	9.6200E-03	-	2.9200E-01	-	2.48
	1.2500E-01	4.5644E-02	1.5000E-03	2.5540	5.9500E-02	2.1862	7.10
	6.2500E-02	2.2451E-02	2.0200E-04	2.8257	9.1500E-03	2.6387	72.45
	3.1250E-02	1.1136E-02	3.0600E-05	2.6917	1.7400E-03	2.3673	1098.16
0.25	2.5000E-01	9.4491E-02	9.5527E-03	-	2.9083E-01	-	1.70
	1.2500E-01	4.5644E-02	1.5118E-03	2.5335	5.9855E-02	2.1726	6.80
	6.2500E-02	2.2451E-02	1.9758E-04	2.8680	9.0223E-03	2.6668	68.94
	3.1250E-02	1.1136E-02	3.0994E-05	2.6419	1.7590E-03	2.3318	1080.45
0.50	2.5000E-01	9.4491E-02	9.5046E-03	-	2.8937E-01	-	1.64
	1.2500E-01	4.5644E-02	1.4746E-03	2.5609	5.8670E-02	2.1931	7.16
	6.2500E-02	2.2451E-02	2.0157E-04	2.8046	9.1130E-03	2.6246	72.51
	3.1250E-02	1.1136E-02	2.9930E-05	2.7202	1.6985E-03	2.3960	1122.41
0.75	2.5000E-01	9.4491E-02	9.5719E-03	-	2.9142E-01	-	1.69
	1.2500E-01	4.5644E-02	1.5000E-03	2.5472	5.9856E-02	2.1753	6.85
	6.2500E-02	2.2451E-02	1.9999E-04	2.8398	9.0586E-03	2.6612	71.37
	3.1250E-02	1.1136E-02	3.0751E-05	2.6703	1.7452E-03	2.3488	1100.52
0.95	2.5000E-01	9.4491E-02	9.6777E-03	-	2.9492E-01	-	1.67
	1.2500E-01	4.5644E-02	1.5392E-03	2.5268	6.1297E-02	2.1590	6.79
	6.2500E-02	2.2451E-02	2.0626E-04	2.8326	9.3339E-03	2.6525	70.67
	3.1250E-02	1.1136E-02	3.0938E-05	2.7058	1.7486E-03	2.3887	1092.28

Table 7. Comparison between the two-grid MVEM and Newton iterative method with $k = 1$.

Mesh	Size	Nodes		Two-grid MVEM	Newton iteration
Voronoi–Lloyd	H:4.4194E-02	1026	$\|\|u - u_h\|\|$	2.7452E-03	2.7452E-03
	h:1.8291E-02	1538	$\|\|\sigma - \sigma_h\|\|$	6.0098E-02	6.0098E-02
			CPU time(s)	10.83	12.77
Distorted Voronoi	H:3.1250E-02	2047	$\|\|u - u_h\|\|$	2.8811E-03	2.8812E-03
	h:1.2886E-02	3071	$\|\|\sigma - \sigma_h\|\|$	6.6545E-02	6.6545E-02
			CPU time(s)	39.17	44.74
Distorted square	H:4.0000E-02	676	$\|\|u - u_h\|\|$	7.4321E-03	7.4323E-03
	h:2.0000E-02	1301	$\|\|\sigma - \sigma_h\|\|$	1.7347E-01	1.7348E-01
			CPU time(s)	5.71	8.88
Non-convex	H:6.2500E-02	769	$\|\|u - u_h\|\|$	8.7996E-03	8.8058E-03
	h:2.2451E-02	1025	$\|\|\sigma - \sigma_h\|\|$	2.2263E-01	2.2267E-01
			CPU time(s)	5.84	6.33

Table 8. Comparison between the two-grid MVEM and Newton iterative method with $k = 2$.

Mesh	Size	Nodes		Two-grid MVEM	Newton iteration
Voronoi–Lloyd	H:4.4194E-02	1026	$\|\|u - u_h\|\|$	5.0281E-05	5.0349E-05
	h:1.8291E-02	1538	$\|\|\sigma - \sigma_h\|\|$	1.0992E-03	1.0998E-03
			CPU time(s)	58.15	92.18
Distorted Voronoi	H:3.1250E-02	2047	$\|\|u - u_h\|\|$	3.7128E-05	3.7213E-05
	h:1.2886E-02	3071	$\|\|\sigma - \sigma_h\|\|$	8.5620E-03	8.5847E-03
			CPU time(s)	208.80	322.90
Distorted square	H:4.0000E-02	676	$\|\|u - u_h\|\|$	1.4867E-05	1.4927E-05
	h:2.0000E-02	1301	$\|\|\sigma - \sigma_h\|\|$	3.4698E-04	3.4787E-04
			CPU time(s)	52.54	107.60
Non-convex	H:6.2500E-02	769	$\|\|u - u_h\|\|$	1.9759E-04	1.9897E-04
	h:2.2451E-02	1025	$\|\|\sigma - \sigma_h\|\|$	4.9982E-03	5.0210E-03
			CPU time(s)	25.54	36.78

As shown in Tables 1 and 5, the two-grid MVEM exhibits more regular and stable numerical performance on the Voronoi-Lloyd meshes. This is because the mesh has better geometric quality, the elements are more regular in shape, and the vertices are distributed more uniformly, which reduces the influence of geometric perturbations on the discretization scheme. For $k = 1$, the convergence order nearly reaches 2 under mesh refinement, while for $k = 2$, the convergence rate approaches the theoretical third-order result. These results confirm that on meshes with good geometric quality, the algorithm achieves convergence behavior closer to theoretical expectations. As can be observed from Tables 4 and 8, the distorted Voronoi meshes generally lead to a larger error than the regular Voronoi-Lloyd meshes. Nevertheless, the proposed method remains numerically stable on these distorted polygonal grids, and the errors still decrease under refinement. Even on non-convex meshes, which pose a more challenging geometric setting for both stability and approximation, the results in Tables 3, 6, 7, and 8 demonstrate that the proposed two-grid MVEM remains reliable for both $k = 1$ and $k = 2$, and the errors decrease consistently under mesh refinement, and the observed convergence rates gradually approach the corresponding theoretical expectations. Meanwhile, although the computational cost increases with the number of degrees of freedom, its growth within a reasonable range. These results indicate that the proposed two-grid MVEM is numerically stable for the problem on geometrically complex polygonal meshes.

In Tables 9–10, we present the numerical results, and CPU time of the two-grid MVEM for different mesh ratios H/h with $k = 1$ and $\alpha = 0.05$ on Voronoi-Lloyd meshes with 64 and 128 elements. For all tested mesh ratios, the proposed two-grid MVEM achieves approximately second-order accuracy for both the variable u and the auxiliary variable σ. As H/h increases from about 2 to 12, the fine-grid errors $||u - u_h||$ and $||\sigma - \sigma_h||$ vary mildly. This indicates that, within the tested range of mesh ratios, the overall error is still dominated by the fine-grid approximation, rather than by the coarse-grid one.

Remark 2. *The Newton method requires repeatedly assembling and solving the linearized coupled discrete system on the refined meshes. Under the experimental settings of this paper, at least three nonlinear iterations are performed per time step, which leads to the fine-grid linear system being solved multiple times. In contrast, the two-grid MVEM constrains the main nonlinear processing on* *the coarse-grid and uses the coarse-grid solution as the initial solution of the fine-grid, so that only one linearized system needs to be solved on the fine-grid, thereby reducing the main computational cost on the fine-grid.*

Table 9. L^2-norm errors of the two-grid MVEM under different mesh ratios H/h with $k = 1$.

H/h	Voronoi-Lloyd 64			H/h	Voronoi-Lloyd 128		
	$\|\|u - u_h\|\|$	$\|\|\sigma - \sigma_h\|\|$	CPU (s)		$\|\|u - u_h\|\|$	$\|\|\sigma - \sigma_h\|\|$	CPU (s)
2.35	2.5248E-02	6.2997E-01	1.84	2.38	1.1283E-02	2.6617E-01	4.44
4.07	2.5951E-02	8.2801E-01	5.73	4.13	1.1400E-02	3.5138E-01	21.18
7.05	2.8098E-02	1.0529E+00	25.87	7.14	1.2320E-02	4.5075E-01	77.17
12.21	2.9731E-02	1.2094E+00	106.86	12.38	1.3031E-02	5.1933E-01	240.82

Table 10. Orders of the two-grid MVEM under different mesh ratios H/h with $k = 1$.

H/h	Voronoi-Lloyd 64		H/h	Voronoi-Lloyd 128		Order	
	H	h		H	h	u	σ
2.35	1.2910E-01	5.4965E-02	2.38	8.8388E-02	3.7113E-02	2.0510	2.1938
4.07	1.2910E-01	3.1734E-02	4.13	8.8388E-02	2.1427E-02	2.0946	2.1827
7.05	1.2910E-01	1.8322E-02	7.14	8.8388E-02	1.2371E-02	2.0993	2.1603
12.21	1.2910E-01	1.0578E-02	12.38	8.8388E-02	7.1425E-03	2.1005	2.1526

6. Conclusion and advancements

In this work, we develop a two-grid MVEM combined with a second-order time approximation scheme for solving the fourth-order time-fractional reaction-diffusion equation with Dirichlet boundary conditions. The original equation is reformulated into a system of second-order equations and the VEM is applied to approximate the spatial direction, providing flexibility in handling complex geometries. We derive the stability of the proposed algorithm and optimal a priori error estimates in L^2-norm. Numerical experiments confirm the accuracy and efficiency of our two-grid MVEM, showing its big potential for complex mesh problems. In future works, we will focus on developing a time two-mesh MVEM by combining the MVEM with the time two-mesh technique [37] for studying high-dimensional problems or incorporating adaptive mesh refinement techniques to further enhance computational efficiency.

Author contributions

Jianmei Chen: Writing-original draft, methodology, formal analysis, software, validation, writing-review & editing; Xinyuan Liu: Formal analysis, writing-review & editing; Yang Liu: Methodology, validation, supervision, funding acquisition, writing-review & editing.

Use of Generative-AI tools declaration

The authors declare that they have not used Artificial Intelligence (AI) tools in the creation of this article.

Acknowledgments

The authors thank the four anonymous reviewers and editors very much for their valuable comments, which greatly helped them to improve this work. This work is supported by the National Natural Science Foundation of China (12461080), Young Innovative Talents Project of Grassland Talents Project, Program for Innovative Research Team in Universities of Inner Mongolia Autonomous Region (NMGIRT2413), and Inner Mongolia Key Laboratory Project of Mathematical Modeling and Scientific Computing (2025KYPT0098).

Conflict of interest

The authors declare that they have no conflict of interest.

References

1. T. F. Feng, Y. Dong, K. L. Zhang, Y. Zhu, Global existence and blow-up to coupled fourth-order parabolic systems arising from modeling epitaxial thin film growth, *Commun. Anal. Mech.*, **17** (2025), 263–289. https://doi.org/10.3934/cam.2025011
2. F. Dekhkonov, W. K. Li, W. P. Wu, On the time-optimal control problem for a fourth order parabolic equation in the three-dimensional space, *Commun. Anal. Mech.*, **17** (2025), 413–428. https://doi.org/10.3934/cam.2025017
3. J. C. Li, Optimal convergence analysis of mixed finite element methods for fourth-order elliptic and parabolic problems, *Numer. Meth. Part. Differ. Equ.*, **22** (2006), 884–896. https://doi.org/10.1002/num.20127
4. C. Wen, J. Wang, Y. Liu, H. Li, Z. Fang, Unconditionally optimal time two-mesh mixed finite element algorithm for a nonlinear fourth-order distributed-order time fractional diffusion equation, *Phys. D*, **460** (2024), 134090. https://doi.org/10.1016/j.physd.2024.134090
5. O. Nikan, J. A. Tenreiro Machado, A. Golbabai, Numerical solution of time-fractional fourth-order reaction-diffusion model arising in composite environments, *Appl. Math. Model.*, **89** (2021), 819–836. https://doi.org/10.1016/j.apm.2020.07.021
6. N. Liu, Y. Liu, H. Li, J. Wang, Time second-order finite difference/finite element algorithm for nonlinear time-fractional diffusion problem with fourth-order derivative term, *Comput. Math. Appl.*, **75** (2018), 3521–3536. https://doi.org/10.1016/j.camwa.2018.02.014
7. M. Haghi, M. Ilati, M. Dehghan, A fourth-order compact difference method for the nonlinear time-fractional fourth-order reaction-diffusion equation, *Eng. Comput.*, **39** (2023), 1329–1340. https://doi.org/10.1007/s00366-021-01524-2

8. X. H. Yang, W. Wang, Z. Y. Zhou, H. X. Zhang, An efficient compact difference method for the fourth-order nonlocal subdiffusion problem, *Taiwan. J. Math.*, **29** (2025), 35–66. https://doi.org/10.11650/tjm/240906
9. Y. Liu, Y. W. Du, H. Li, J. Li, S. He, A two-grid mixed finite element method for a nonlinear fourth-order reaction-diffusion problem with time-fractional derivative, *Comput. Math. Appl.*, **70** (2015), 2474–2492. https://doi.org/10.1016/j.camwa.2015.09.012
10. J. Guo, Q. Pan, D. Xu, W. Qiu, A spectral order method for solving the nonlinear fourth-order time-fractional problem, *J. Appl. Math. Comput.*, **68** (2022), 4645–4667. https://doi.org/10.1007/s12190-022-01719-w
11. P. Roul, V. P. Goura, A high order numerical method and its convergence for time-fractional fourth order partial differential equations, *Appl. Math. Comput.*, **366** (2020), 124727. https://doi.org/10.1016/j.amc.2019.124727
12. X. H. Yang, Z. M. Zhang, Superconvergence analysis of a robust orthogonal Gauss collocation method for 2D fourth-order subdiffusion equations, *J. Sci. Comput.*, **100** (2024), 62. https://doi.org/10.1007/s10915-024-02616-z
13. M. Abbaszadeh, M. Dehghan, Direct meshless local Petrov-Galerkin (DMLPG) method for time-fractional fourth-order reaction-diffusion problem on complex domains, *Comput. Math. Appl.*, **79** (2020), 876–888. https://doi.org/10.1016/j.camwa.2019.08.001
14. L. Beirão da Veiga, F. Brezzi, A. Cangiani, G. Manzini, L. D. Marini, A. Russo, Basic principles of virtual element methods, *Math. Model. Meth. Appl. Sci.*, **23** (2013), 199–214. https://doi.org/10.1142/S0218202512500492
15. L. Beirão da Veiga, F. Brezzi, L. D. Marini, A. Russo, The hitchhiker's guide to the virtual element method, *Math. Model. Meth. Appl. Sci.*, **24** (2014), 1541–1573. https://doi.org/10.1142/S021820251440003X
16. F. Brezzi, R. S. Falk, L. D. Marini, Basic principles of mixed virtual element methods, *ESAIM: Math. Model. Numer. Anal.,* **48** (2014), 1227–1240. https://doi.org/10.1051/m2an/2013138
17. G. Vacca, L. Beirão da Veiga, Virtual element methods for parabolic problems on polygonal meshes, *Numer. Meth. Part. Differ. Equ.*, **31** (2015), 2110–2134. https://doi.org/10.1002/num.21982
18. D. Adak, E. Natarajan, S. Kumar, Convergence analysis of virtual element methods for semilinear parabolic problems on polygonal meshes, *Numer. Meth. Part. Differ. Equ.*, **35** (2019), 222–245. https://doi.org/10.1002/num.22298
19. M. Li, J. Zhao, Z. Wang, S. Chen, Conservative conforming and nonconforming VEMs for fourth order nonlinear Schrödinger equations with trapped term, *J. Comput. Math.*, **42** (2024), 454–499. https://doi.org/10.4208/jcm.2209-m2021-0038
20. L. Pei, C. Zhang, M. Li, Dissipative nonconforming virtual element method for the fourth order nonlinear extended Fisher-Kolmogorov equation, *Comput. Math. Appl.*, **152** (2023), 28–45. https://doi.org/10.1016/j.camwa.2023.10.007

21. M. Li, J. Zhao, C. Huang, S. Chen, Conforming and nonconforming VEMs for the fourth-order reaction-subdiffusion equation: a unified framework, *IMA J. Numer. Anal.*, **42** (2022), 2238–2300. https://doi.org/10.1093/imanum/drab030
22. Y. Zhang, M. Feng, A mixed virtual element method for the time-fractional fourth-order subdiffusion equation, *Numer. Algor.*, **90** (2022), 1617–1637. https://doi.org/10.1007/s11075-021-01244-0
23. J. C. Xu, Iterative methods by space decomposition and subspace correction, *SIAM Rev.*, **34** (1992), 581–613. https://doi.org/10.1137/1034116
24. J. C. Xu, A novel two-grid method for semilinear elliptic equations, *SIAM J. Sci. Comput.*, **15** (1994), 231–237. https://doi.org/10.1137/0915016
25. Q. Gu, Y. P. Chen, J. Zhou, Y. Huang, A two-grid virtual element method for nonlinear variable-order time-fractional diffusion equation on polygonal meshes, *Int. J. Comput. Math.*, **100** (2023), 2124–2139. https://doi.org/10.1080/00207160.2023.2263589
26. Y. Zeng, Y. Li, Y. Zeng, Y. Cai, Z. Luo, The dimension reduction method of two-grid Crank-Nicolson mixed finite element solution coefficient vectors for nonlinear fourth-order reaction diffusion equation with temporal fractional derivative, *Commun. Nonlinear Sci. Numer. Simulat.*, **133** (2024), 107962. https://doi.org/10.1016/j.cnsns.2024.107962
27. D. X. Wang, Y. N. Li, H. E. Jia, A two-grid finite element method for the Allen-Cahn equation with the logarithmic potential, *Numer. Meth. Part. Differ. Equ.*, **39** (2023), 1251–1265. https://doi.org/10.1002/num.22932
28. X. Y. Liu, N. Liu, Y. Liu, H. Li, Analysis of variable-time-step BDF2 combined with the fast two-grid finite element algorithm for the Fitzhugh-Nagumo model, *Comput. Math. Appl.*, **170** (2024), 186–203. https://doi.org/10.1016/j.camwa.2024.07.001
29. G. H. Gao, H. W. Sun, Z. Z. Sun, Stability and convergence of finite difference schemes for a class of time-fractional sub-diffusion equations based on certain superconvergence, *J. Comput. Phys.*, **280** (2015), 510–528. https://doi.org/10.1016/j.jcp.2014.09.033
30. Y. J. Wang, Y. Liu, H. Li, J. F. Wang, Finite element method combined with second-order time discrete scheme for nonlinear fractional cable equation, *Eur. Phys. J. Plus*, **131** (2016), 61. https://doi.org/10.1140/epjp/i2016-16061-3
31. K. Hormann, M. S. Floater, Mean value coordinates for arbitrary planar polygons, *ACM Trans. Graph.*, **25** (2006), 1424–1441. https://doi.org/10.1145/1183287.1183295
32. H. Sun, Z. Z. Sun, G. H. Gao, Some temporal second order difference schemes for fractional wave equations, *Numer. Meth. Part. Differ. Equ.*, **32** (2016), 970–1001. https://doi.org/10.1002/num.22038
33. Q. F. Li, Y. P. Chen, Y. Q. Huang, Y. Wang, Two-grid methods for nonlinear time fractional diffusion equations by $L1$-Galerkin FEM, *Math. Comput. Simulat.*, **185** (2021), 436–451. https://doi.org/10.1016/j.matcom.2020.12.033
34. Y. H. Zeng, Z. J. Tan, Two-grid finite element methods for nonlinear time fractional variable coefficient diffusion equations, *Appl. Math. Comput.*, **434** (2022), 127408. https://doi.org/10.1016/j.amc.2022.127408

35. S. C. Brenner, L. R. Scott, *The mathematical theory of finite element methods*, 3^{rd} edition, Springer, New York, 2008. https://doi.org/10.1007/978-1-4757-4338-8

36. C. Talischi, G. H. Paulino, A. Pereira, I. F. M. Menezes, PolyMesher: a general-purpose mesh generator for polygonal elements written in Matlab, *Struct. Multidiscip. Optim.*, **45** (2012), 309–328. https://doi.org/10.1007/s00158-011-0706-z

37. Y. N. Yang, C. Wen, Y. Liu, H. Li, J. F. Wang, Optimal time two-mesh mixed finite element method for a nonlinear fractional hyperbolic wave model, *Commun. Anal. Mech.*, **16** (2024), 24–52. https://doi.org/10.3934/cam.2024002